*J. Fluid Mech.* (1987), *vol.* 180, *pp.* 193–229
*Printed in Great Britain*



# Eduction of large-scale organized structures in a turbulent plane wake

By A. K. M. FAZLE HUSSAIN AND M. HAYAKAWA†
Department of Mechanical Engineering, University of Houston, Houston, TX 77004, USA

(Received 25 February 1986 and in revised form 25 November 1986)

Large-scale organized structures in the turbulent plane wake of a circular cylinder are investigated in air up to a downstream distance of $40d$ at a Reynolds number of $Re_d = 1.3 \times 10^4$; $d$ is the cylinder diameter. Velocity signals from a linear transverse rake of 8 X-wires are sampled simultaneously to calculate the instantaneous spanwise vorticity. We have appropriately smoothed the temporal traces of vorticity to obtain time evolutions (including the transverse displacement, sign, strength and size distributions) of organized structures identified by vorticity contour maps. The periodicity of the initial structures is rapidly lost: dispersion in streamwise spacing, transverse displacement, strength and size of structures increases with increasing downstream distance.

Particular emphasis is placed on examining alternative general schemes for educing coherent structures in natural or unexcited turbulent shear flows, especially in their fully developed states. The optimal eduction scheme employed involves centring the rake at the most probable transverse location of centres of advected structures and accepting those structures that: (i) are centred at the midpoint of the rake, (ii) have a peak value of (smoothed) vorticity of a given sign above a specified level, and (iii) have streamwise and transverse extents of the (smoothed) vorticity contours above a specified size. From successive accepted structure signatures the instants of occurrence of structure centres (i.e. smoothed vorticity peaks) are identified. *Unsmoothed* signals are then time-aligned with respect to these instants and ensemble averaged to educe coherent structure and incoherent turbulence characteristics. Further enhancement is achieved by iteratively improving the time-alignment by maximizing the cross-correlation of individual structure vorticity with the ensemble-averaged vorticity and by discarding structures that require excessive time shifts or that produce significantly weak peak correlation values.

Following this optimal scheme, large-scale coherent structures have been educed in the fully turbulent wake. The average structure centre is found to be closer to the wake centreline than the half-width location, and the structure size does not increase in proportion to the wake width, suggesting that transverse wandering of structures (including their three-dimensionality) increases significantly with increasing downstream distance. The various flow properties associated with coherent and incoherent turbulence, and the coherent structure dynamics, in particular the role of vortex stretching (at the saddle) in turbulence production and mixing, are discussed.

---

† Permanent address: Department of Mechanical Engineering II, Hokkaido University, Sapporo 060, Japan.

## 1. Introduction

In spite of widespread contemporary interest in coherent structures, there have been very few quantitative measurements capturing topological details of these structures or elucidating their dynamical role or significance. Since the concept of a coherent structure intuitively implies a spatial description of the instantaneous flow field and time evolutions of spatial flow patterns, flow visualization has played an important role in coherent-structure studies (for example, Kline *et al.* 1967; Crow & Champagne 1971; Brown & Roshko 1974; Winant & Browand 1974). However, lack of quantitative data in these studies regarding instantaneous spatial details of structures has prevented the understanding of the flow physics. In fact, flow visualization can even be misleading at times; for example, smoke lumps observed in the far wake of a cylinder (at low Reynolds numbers, say, $Re_d \approx 140$) can be easily misinterpreted as shed vortices (Taneda 1959; Cimbala 1984), even though it should have been obvious that because of the large 'effective' Schmidt number, vorticity diffuses away from the smoke lumps much sooner than recognized before (Tritton 1959; Zdravkovich 1968). Although image-processing techniques appear highly promising for simultaneous visualization and quantitative measurement of the time-dependent spatial structure of turbulence, these techniques are still in their infancy, being under development in numerous laboratories including ours.

In quantitative measurements of organized structures, the most extensively used technique so far has been periodic sampling applied to flows which are either subjected to controlled excitation or characterized by an inherent periodicity. This kind of measurements has shown great success in jets under controlled excitation (Hussain 1981*a*), in the near wake (Cantwell & Coles 1983, hereinafter referred to as CC) and in the artificially produced 'turbulent spot' in a turbulent environment (Zilberman, Wygnanski & Kaplan 1977; Kleis, Hussain & Sokolov 1981). However, such phase-locked measurements are useful only in the region where the marked periodicity of the flow is retained. Their usefulness is progressively lost, owing to increasing jitter, with increasing distances from the region where structure formation is induced by the periodic excitation. The effect of this jitter can be reduced by triggering structure eduction on a signal obtained from a reference probe at the measurement station even when excitation is used (see, for example, Hussain & Zaman 1980) or by alignment via optimization of correlation of a measurement signal with an upstream reference signal (see Kleis *et al.* 1981), rather than triggering on an upstream reference signal (see CC, for example).

Eduction of natural or unforced coherent structures has been pursued mostly in mixing layers where the characteristic velocity signature at the edge of the shear layer, caused by the passage of large-scale structures, was used as a trigger signal (Browand & Weidman 1976; Bruun 1977; Yule 1978; Zaman & Hussain 1984). Hussain & Zaman (1982) optimized a single-point triggering technique to educe topological details of structures in the developing and self-preserving regions of a high-Reynolds-number, initially fully turbulent plane mixing layer.

It should be mentioned, however, that an eduction method triggered on the velocity signals outside a structure has some limitations. For example, this method cannot discriminate the velocity signature of a weaker structure passing near the trigger probe from that of a stronger structure advecting farther away from the probe. Thus, eduction using a trigger based on a footprint signature from outside the structures can produce excessive smearing of the topological details of structures as a result of ensemble averaging of different kinds of structures sampled by such a trigger. Eduction of coherent structures in natural (i.e. unexcited) flows or in fully developed

turbulent states of even excited flows must rely upon more sophisticated conditional-sampling measurements involving three-dimensional pattern recognition and signal-enhancement techniques.

Recent three-dimensional numerical simulation of a plane mixing layer (Metcalfe *et al.* 1987) revealed that even the large-scale spanwise roll structure in the plane mixing layer is considerably more three-dimensional than implied by hot-wire and flow-visualization studies (Browand & Troutt 1985; Breidenthal 1980). The three-dimensionality is to be expected because of the occurrence of longitudinal vortices or coherent substructures (for example, 'ribs' (see Hussain 1983*b*) which induce spanwise contortions of rolls). The so-called spanwise rolls in a mixing layer do indeed consist of highly contorted substructures, as has been amply demonstrated by numerous flow-visualization studies (see also Bernal 1981; Jimenez, Cogollos & Bernal 1985). A detection using a trigger based on a velocity signal from the edge of a turbulent shear flow will capture only the overall 'footprint', but miss the internal details of structures. Also, a point detection cannot uniquely discriminate differences between structures of different shapes and sizes; for example, a point detection cannot distinguish a large structure moving rapidly and a small structure moving slowly. Thus, a point detection is likely to produce significant smearing and distorted perception of the flow physics. It is not surprising that single-sensor detection of three-dimensional (random) structures, even via sophisticated conditional-sampling measurements, has produced highly smeared educed signatures with little relevance to the instantaneous structures (Blackwelder & Kaplan 1976; Nishioka, Asai & Iida 1981) and with structure characteristics highly sensitive to the details of the eduction criteria (Sato 1983; Kunen, Ooms & Vink 1983).

The present work was motivated by the fact that the topological details of the plane wake structure is completely unknown and that Grant's (1958) 'double roller' structure is quite in contrast to the intuitive picture of a cylinder wake structure. We believe that coherent structures should be characterized by large-scale vorticity concentrations (i.e. high values of smoothed vorticity field). Thus, the least ambiguous quantity for the recognition of structures should be the vorticity itself (Hussain 1981*a*, 1983*a*). This method has the advantage that it requires neither a periodic reference signal nor a trigger signal, but relies on the measurement signal itself, thus eliminating any ambiguity in the detection of a structure as well as its size, location, strength, etc. With this in mind, we used a rake of X-wires and calculated the instantaneous spanwise (large-scale) vorticity from which coherent structures are identified as those with large-scale vorticity concentrations. A similar technique has been used by Tso (1983) in our laboratory to examine large-scale structures of different modal shapes in the far field of a turbulent circular jet.

The present measurements were made in the turbulent plane wake behind a circular cylinder placed normal to the flow. Because of its simple geometry and relevance to various practical applications, the cylinder wake has attracted continuing attention of numerous researchers since the early part of this century (see Townsend 1956). The plane wake flow has been recently revisited by many investigators from the point of view of coherent structures. Townsend (1979) has examined the far-wake region by means of an array of single hot wires. Short-time correlation of longitudinal velocities with a 'template' pattern was used to infer passages of different assumed structure patterns. Using a similar approach, Mumford (1983) has demonstrated that several modes of large eddies occur in the self-preserving region. The plane wake has been further studied not only regarding its self-preservation (Sreenivasan & Narasimha 1982; Wygnanski, Champagne & Marasli 1986) but also its near-field structure evolution (Wlezien 1981; Boisson 1983). However, in spite of these recent

efforts, the shape of the coherent structure in a cylinder wake, let alone its topological details and dynamical significance, is still speculative, and the understanding of the flow physics is grossly unsatisfactory. Compared to other free shear flows, the most pronounced feature of the wake is the initial formation of fairly organized, alternating and nearly two-dimensional spanwise vortices (the so-called Kármán vortex street), although the shedding is not always parallel to the cylinder (Tritton 1959; Gerrard 1966; Nishioka & Sato 1978; Cimbala 1984). Because of the periodic formation of structures, the near wake flow is a fertile ground for fundamental studies of topological details of coherent structures in general and their dynamical roles. In fact, utilizing this advantage, CC made extensive measurements by 'the flying-hot-wire technique' in the near wake up to $8d$ at the Reynolds number of $Re_d = 1.4 \times 10^5$; the data sampling was triggered on the periodic static pressure variation on the cylinder surface. However, this upstream-trigger method for eduction appears to us to have involved jittering effect, which is increasingly significant with increasing $x$. D. Coles (1984, private communication) has mentioned extreme difficulty in educing the wake structure beyond the first few diameters. Clearly, eduction in a turbulent flow can suffer from smearing due to two factors: initiation and evolutionary jitters. Eduction based on an upstream signal that characterizes structure initiation can eliminate initiation jitter but cannot avoid evolutionary (including trajectory) jitter inherent in all turbulent flows.

The present attempt is based on a new, and we believe a universal, eduction scheme which uses the local measurement signal itself for trigger without requiring a reference (external) signal. As such, this new eduction scheme suffers from minimal jitter and is effective in capturing the topological details of structures, and the scheme is suitable for any – particularly unexcited – fully turbulent flow. The measurements here cover the streamwise stations $x/d = 10$, 20, 30 and 40. We selected this $x$-range because the initially shed vortices disintegrate by a downstream distance of about $x/d = 50$ to 100 (Roshko 1954; Taneda 1959; Zdravkovich 1968; Keffer 1965; Durgin & Karlsson 1971). Furthermore, the mechanism or location for full development of newer structures formed farther downstream is not known; and we do not know that these newer, downstream structures resemble those nearer the cylinder. We consider this $x$-range to be adequate in demonstrating the success of the eduction scheme, which can easily be applied in the far wake and in any fully turbulent flow.

The eduction technique and the results discussed in this paper have been previously presented by us (Hayakawa *et al.* 1983; Hayakawa & Hussain 1985).

## 2. Experimental set-up

The experiments were conducted in an open-return, low-turbulence wind tunnel with a test section of 92 cm × 46 cm cross-section and 8 m working length. A 2.7 cm diameter rigid circular cylinder (solid aluminum rod) with a hydrodynamically smooth surface was installed parallel to the 92 cm side on the centreline of the test section, resulting in a low blockage (6%) and an adequate aspect ratio of 32. A linear array of eight X-wire probes was mounted on a traversing mechanism, which was remotely controlled by a minicomputer located outside the test room. A 16-channel home-made anemometer set (adapted from USC design) was used for velocity measurements. The voltage signals from the anemometers were sampled via a 12-bit A/D converter and stored on digital magnetic tapes for later analysis. The total sampling rate of 20 KHz, that is 1.25 KHz for each channel, was considered adequate for the eduction of large-scale structures.

All data were taken at a constant free-stream velocity of $U_0 = 7$ ms$^{-1}$. The Reynolds number $Re_d$ based on the cylinder diameter $d$ was $1.3 \times 10^4$, well within the subcritical flow regime with laminar separation and a constant shedding Strouhal number of 0.21. Under this flow condition, the vortex-shedding frequency $f_s$ on a side of the wake was 54 Hz. The probe setting was adjusted such that its spatial range covered at least the transverse extent of typical structures (discussed later). Except for the case of additional measurements at $x/d = 20$, the spatial separation between adjacent X-probes was 1 cm.

## 3. Eduction method

### 3.1. *Detection quantity*

Since a coherent structure is a large-scale organized motion of turbulent fluid with coherent (i.e. spatially phase-correlated instantaneous) vorticity concentration, vorticity is the optimal quantity needed to identify the coherent structure (Hussain 1981*a*, 1983*a*). The structure, especially in the fully turbulent wake, is expected to be three-dimensional. Thus, in principle, a three-dimensional array of vorticity sensors is needed for the detection and eduction of coherent structures. The cost and limitations of current measurement technology render such a detection scheme prohibitive, and hence one has to settle for a simpler, less-rigorous detection scheme. Thus, the spanwise component of vorticity (in the plane of the rake of X-wires and the flow direction) was used as the detection quantity for structure-passage identification.

For an array of X-wires in the $(x, y)$-plane with a spatial separation of $\Delta S$ between adjacent probes, we have instantaneous velocity signals, $u$ (streamwise) and $v$ (transverse), at discrete $y$-locations, and thus the spanwise component of vorticity $\omega$ is approximated by

$$\omega = \frac{\partial v}{\partial x} - \frac{\partial u}{\partial y} \approx -\frac{1}{U_c}\frac{\Delta v}{\Delta t} - \frac{\Delta u}{\Delta S}, \tag{1}$$

where $\Delta t$ is the timestep between successive data points. Note that (1) invokes Taylor's hypothesis with $U_c$ as the structure advection velocity. Zaman & Hussain (1981) showed that, despite theoretical predictions to the contrary, this hypothesis works well for coherent structure measures, particularly involving isolated structures with no intense interaction like pairing or tearing, provided that the advection velocity of the structure centre is used for $U_c$ (in (1)), everywhere across a shear flow. In situations where the structure advection velocity is not known, they suggested that use of a single advection velocity everywhere across the shear flow and equal to an average of velocities across the shear region is the least objectionable choice. On this basis, the velocity at the half-velocity-defect point (i.e. $y = b$) was used initially for $U_c$. However, our measurements showed that the average location for centres of passing structures is shifted considerably in the transverse direction from the $y = b$ line (see §4.1). Therefore, we used the measured structure advection velocity (from vorticity correlation between two $x$-stations) as the final choice for $U_c$ in the computation of coherent vorticity (equation (1)) and other coherent-structure properties.

In the computation of vorticity, the central-difference approximation was used so that the array of eight X-wires gave the instantaneous vorticity at seven intermediate locations of the rake, i.e. at midpoints between two neighbouring X-wires. For example, considering two adjacent $y$-locations, $y_1$ and $y_2$, and two successive time

instants, $t_1$ and $t_2$, we have four instantaneous velocity signals for $u$ and $v$, respectively. From these, the vorticity at the central point A is computed with a linear approximation as

$$\omega_A = \frac{1}{U_c \Delta t}\left\{\frac{v_{21}+v_{11}}{2} - \frac{v_{22}+v_{12}}{2}\right\} - \frac{1}{\Delta S}\left\{\frac{u_{22}+u_{21}}{2} - \frac{u_{12}+u_{11}}{2}\right\},$$

where the first subscript denotes the $y$-location and the second subscript denotes the instant of time. The unavoidable smoothing in this process due to finite transverse probe spacing as well as the slow data sampling rate is acceptable for large-scale structure eduction. Note that all structure properties are finally educed from *unsmoothed* hot-wire signals directly. That is, the *smoothed* vorticity maps merely facilitate the identification of underlying structures and their centres, but do not affect the educed structure details for which unsmoothed signals are used. Thus, incoherent turbulence measures, though obtained at discrete points, are free from effects of smoothing.

Because our primary interest is in large-scale events, the recognition of structures was performed on the basis of smoothed, instantaneous vorticity signals which were obtained by the short-time-averaging technique. The short-time average $\tilde{f}$ of a temporal quantity $f(t)$ is defined as

$$\tilde{f}(t;T) = \frac{1}{T}\int_{t-\frac{1}{2}T}^{t+\frac{1}{2}T} f(t')\,\mathrm{d}t',$$

where $T$ is the interval for averaging and $t$ is the instant to which the short-time-averaged value is assigned. This smoothing is equivalent to low-pass filtering without any phase shift, or equivalently, convolving a noisy function $f(t)$ with a smoothing filter whose impulse response is a rectangular pulse of duration $T$ and height $1/T$. In a flow where Taylor's hypothesis is applicable, the $f \rightarrow \tilde{f}$ mapping corresponds to a spatial smoothing of the local, temporal event. The choice of $T$ is arbitrary to some extent. However, $T$ should be chosen to be smaller than, but of the same order as, the average time between passages of large-scale structures so that this averaging smooths out the high-frequency (mostly incoherent) fluctuations but retains the underlying large-scale vorticity. In the present analysis, $T$ was chosen as about $\frac{1}{7}T_s$, $T_s$ being the mean vortex passage interval on a side of the wake; i.e. $T_s = 1/f_s$.

### 3.2. *Instantaneous vorticity field*

In order to demonstrate the existence of large-scale structures as well as to obtain a qualitative perception of the instantaneous flow, we have examined, first, a number of smoothed vorticity contours; some examples are shown in figures 1 (*a–d*) for three $x$-stations. For reference, the (smoothed) contours of $u$ and $v$ corresponding to figures 1 (*a*) and (*d*) are shown in figures 2 (*a*, *b*) and 2 (*c*, *d*), respectively. The time lapse is taken from right to left, and the ordinate is non-dimensionalized by $b$ (i.e. $Y = y/b$); where $b$ is the wake half-width defined on the basis of the mean velocity profile $U(y)$, as usual. If time is transformed into streamwise distance by assuming $x = -U_c t$, the abscissa scale corresponds to about $\frac{1}{5}$th of the transverse scale. That is, the streamwise coordinate in figures 1 and 2 is compressed 5 times to include more structures. In the vorticity maps (figures 1 *a–d*), contour levels are normalized by the local maximum mean shear, $S_M \equiv (\partial U/\partial y)_{max}$; clockwise and counterclockwise vorticity levels are denoted by broken and solid lines, respectively. These figures do not show spatial

growth of the structures, but provide instantaneously occurring, temporal events at fixed spatial stations. However, because structure evolution is rather slow, the time evolution of vorticity gives a reasonable approximation of the spatial pattern at around the measurement station; the $x = -U_c t$ transformation is obviously tenuous at large $x$ or $t$. The centre of the rake was appropriately shifted away from the wake centreline for each $x$-station but the transverse extent covered by the rake was the same at all $x$-stations because of the fixed probe separation. Thus, the transverse extent relative to the wake width decreases downstream. These contour maps 'visualize' reasonably well the instantaneous structures.

At the farthest upstream position, i.e. $x = 10d$, one can recognize alternating vortices with similar cross-sections. Nevertheless, some irregularities like transverse displacement and elongation of vortex (for example, those marked as D and E in figure 1 *a*) are already observed. This contrasts somewhat to the usual perception of shed vortices (e.g. two-dimensional and periodic) based on only a single-sensor velocity signal or flow visualization. (We note in passing that it is very unlikely that a single observable can be used to characterize an open flow (K. R. Sreenivasan 1984, private communication). We feel that any signal interpretation of open flows in terms of chaos must be accompanied by flow visualization and careful hydrodynamical interpretation.) Note that most vortex centres are located much closer to the wake centreline than the half-velocity-defect point (i.e. $y = b$). The structure irregularity increases with the downstream distance. At $x = 20d$, structures still occur relatively regularly for some intervals but quite irregularly at other intervals; figures 1 (*b*, *c*) are shown as two extreme examples. Such non-uniformities are in striking contrast with periodic smoke or dye lumps shown in flow visualization and may be related to unsteadiness in the initial formation of vortices; this has been observed as low-frequency amplitude modulation in velocity or pressure signature near the separation point (for example, see figure 4 of CC). The wake structure periodicity tends to disappear with increasing $x$. At the last station, i.e. $x = 40d$, the distortion of structures becomes more prominent. The appearance of smaller- (i.e. intermediate-) scale structures suggests the occurrence of significant tearing, perhaps due to evolution of three-dimensionality, and there are frequent excursions of structures across the wake centreline (figure 1 *d*). Additional realizations of the vorticity map at $x/d = 40$ are shown in figures 1 (*e–g*); these are helpful in obtaining a reliable perception of the far-field wake structure. With increasing distance from the cylinder, there is increasing dispersion in structure size, strength, transverse displacement, longitudinal spacing, etc. While vortices are shed alternately and are initially of equal strengths on the two sides (figure 1 *a*), the adjacent vortices farther downstream are not necessarily of opposite signs, and their strengths vary widely (figures 1 *d–g*). Thus, if eduction is triggered on the initial vortex-shedding event (see CC), the educed structures will suffer from significant smearing owing to the streamwise and transverse wandering of structures, to inclusion of structures of different characteristic measures, and to cancellation of vorticity of opposite signs. To elaborate, eduction based on the oscillating surface pressure on the cylinder surface can eliminate jitter in structure initiation but not the inherent jitter in structure evolution and trajectory. From the decrease of circulation with increasing $x$ observed in their measurements, CC suggested annihilation of vorticity owing to migration across the wake centreline. Clearly, eduction based on an upstream signal can result in loss of ensemble-averaged circulation without any annihilation of vorticity of individual structures necessarily being involved. Our eduction method is free from this problem evident in CC's data.

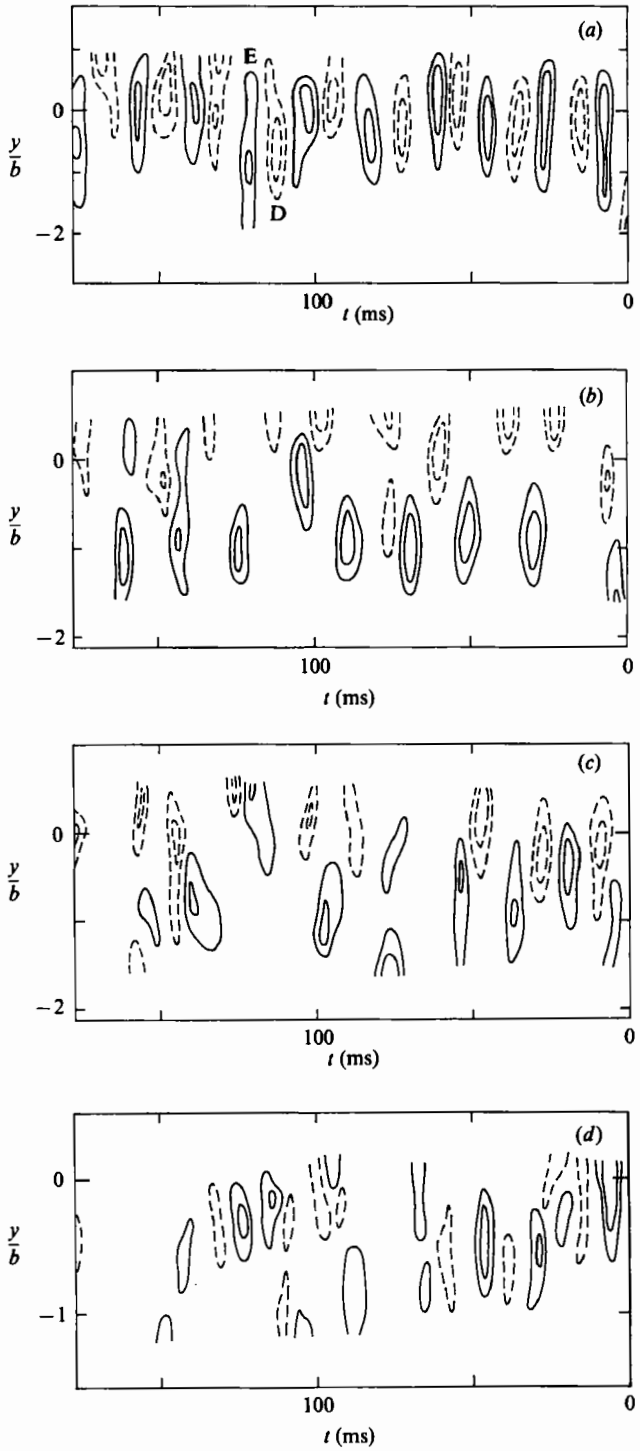


FIGURE 1 (*a–d*). For caption see facing page.

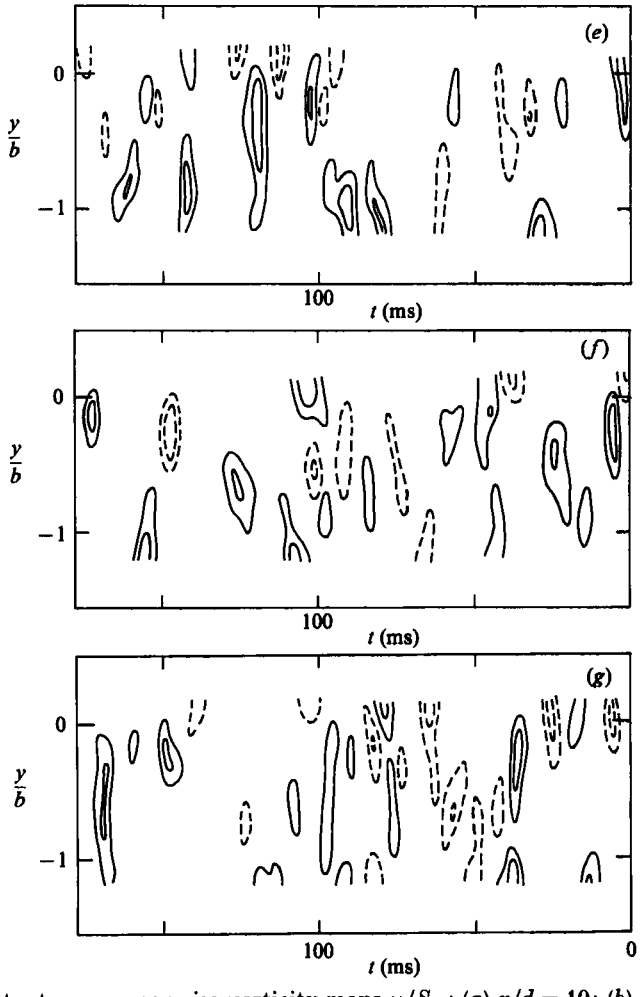


FIGURE 1. Instantaneous spanwise vorticity maps $\omega/S_M$; (*a*) $x/d = 10$; (*b*) 20; (*c*) 20; (*d*)–(*g*) 40; contour levels: 5.0, 2.5.

It is apparent from the vorticity maps (figures 1*a–g*) that the shed vortices do not exhibit a substantial growth in size in proportion to the spreading of the wake. Note again that contour levels are non-dimensionalized by the local quantity $S_M$ which decreases downstream. There are some larger vortices like the ones at $t \approx 120$ ms in figure 1(*e*) and $t \approx 170$ ms in figure 1(*g*), but such are actually very rare events. Our data suggest that the spreading of the turbulent wake cannot be attributed directly to structure growth. Note also that the percentage of structures of a size that is comparable to the local wake width decreases with increasing $x$. These features may be due to increasing transverse wandering and three-dimensionality of structures, due to evolution of 'ribs' as well as due to the occurrence of tearing, but have not been addressed so far even by visualization studies. Although a typical flow-visualization effort tracks the time evolution of vorticity-bearing markers, thus producing streaklines which give an integral effect of the history of motion of the markers, the boundary of the smoke- or dye-marked fluid departs progressively from the vorticity

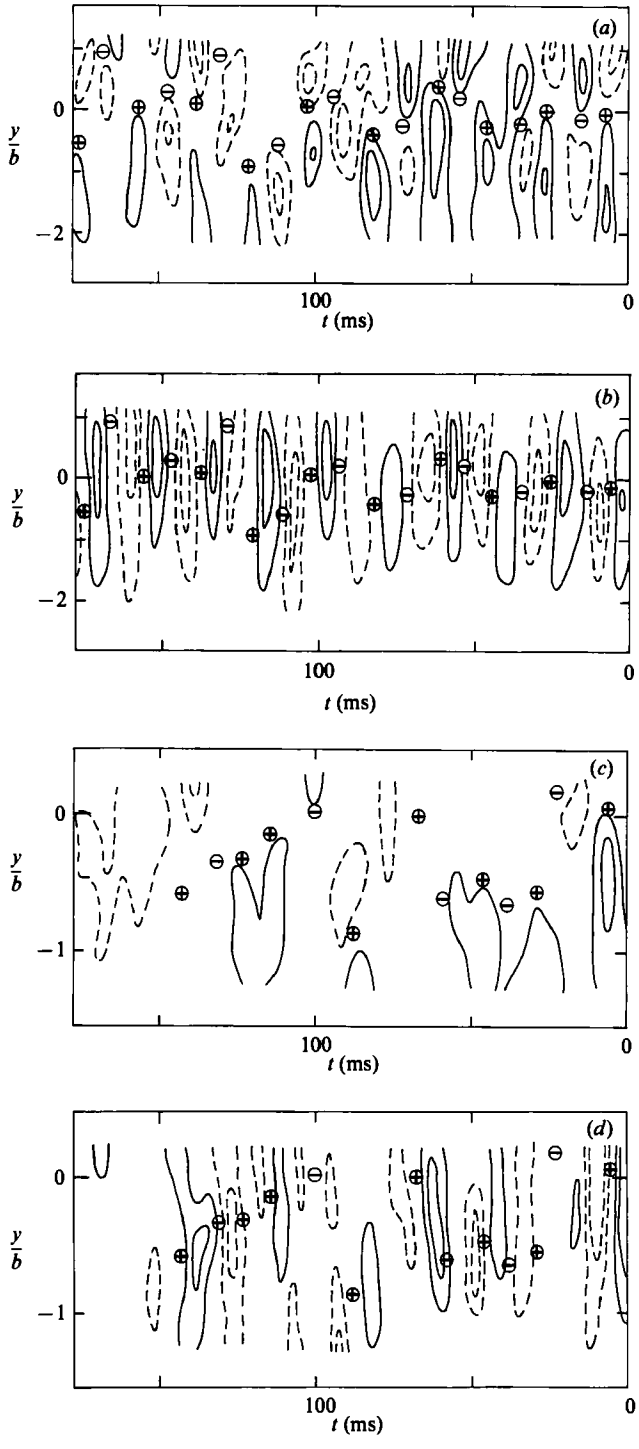


FIGURE 2. Instantaneous velocity maps; (*a*) $u/U_0$ at $x/d = 10$; (*b*) $v/U_0$ at $x/d = 10$; levels: 0.2, 0.1; (*c*) $u/U_0$ at $x/d = 40$; (*d*) $v/U_0$ at $x/d = 40$; levels: 0.1, 0.05.

boundary with increasing downstream distance because of the large (effective) Schmidt number. Thus, flow visualization does not usually depict local events everywhere. Since the markers can be assumed to faithfully track fluid particles for short intervals after their release, it is desirable, though typically impractical, to release markers locally at the point of interest in the flow. In this sense, hydrogen-bubble wire (in water) and smoke wire (in air) are particularly attractive. More promising for instantaneous flow-field measurement in the three-dimensional space are techniques that are yet to be developed or perfected: for example, pulsed laser holography, laser-induced fluorescence velocimetry, NMR imaging and ESR imaging. The time-dependent spatial events in the flow can be captured far more unambiguously by the local instantaneous vorticity maps; hence the thrust of the present study.

Figures 2(*a–d*) provide interesting details of the (smoothed) velocity perturbation fields, which may be attributed to coherent structures. The corresponding structure centres along with the sign, as inferred from figure 1, are also indicated. These velocity fields are included to re-emphasize the point that structures and their boundaries cannot be detected from $u$, $v$ or intermittency signals. For example, the vorticity field is unique for a given velocity field and not vice versa, and intermittency contours extend beyond structure boundary. Note that it is a unique situation only in the case of the 'spot' in a laminar boundary layer that the velocity perturbation boundary closely resembles the structure boundary (Wygnanski, Sokolov & Friedman 1976; Cantwell, Coles & Dimotakis 1978). However, a number of coherent-structure investigations in turbulent shear flows have been based on velocity-perturbation signals only (for example, Townsend 1979; Mumford 1983). The $u$-, $v$-contours (for example, figure 2*c*) demonstrate that these flow quantities are poorer identifiers of coherent structures, a point repeatedly emphasized previously (Hussain 1981*a*, 1983*a*).

Townsend (1979) has claimed that periodic flow patterns resembling a Kármán vortex street occur in a fully turbulent wake (at $Re_d = 8000$), that groups of three to five structures occur at a time, that the period within each group is constant but varies from one group to another, and that random fluctuations fill in the space between the groups (see also Mumford 1983). Gupta, Laufer & Kaplan (1971) made a similar claim for organized structures near the wall of a turbulent boundary layer. Such periodicity is apparent in the left-hand side of figure 1(*e*) and in the right-hand side of figures 1(*b, c, f*). However, organized flows (with coherent structures embedded in them) still occur in between the groups of periodic structures with irregular spacing, size and transverse displacements. Townsend, Mumford and Gupta *et al.* could not detect such structures because their measurements were all obtained by $u$-velocity probes only.

Wlezien (1981) suggested that with increasing $x$ the structures moved closer to the wake centreline. There are occasions when this may appear to be true, but no such trend is apparent as a rule.

Matsui & Okude (1981, 1983) have claimed on the basis of both flow visualization and hot-wire measurements that wake structures undergo pairing, while Cimbala, Nagib & Roshko (1981) and Desruelle (1983) contested this claim and supported the conjecture of Taneda (1959) that the newer structure was the result of instability of the turbulent wake. There is no evidence of strong pairing activity from figures 1 and 2. Because pairing typically occurs between vortices of the same circulation, one would not expect pairing to occur in a wake. (As an aside, H. S. Husain (1984) has shown pairing between opposite-signed vortices of different circulation strengths in

the near field of a plane jet in our laboratory.) However, if two adjacent structures happen to be of the same circulation sign (for example, at $t \approx 120$ ms in figure 1*d* and at $t \approx 80$ ms in figure 1*e*), pairing is likely to occur and should not be surprising, even though pairing cannot be a dominant activity in the wake. Note that at $x/d = 40$ not all structures have decayed uniformly: structures at $t \approx 45$ ms in figure 1 (*d*) and $t \approx 120$ ms in figure 1 (*e*) are relatively strong while others have decayed, perhaps via tearing and partial pairing (discussed by Hussain & Clark 1981). The strong structures are fewer at larger $x$ while the fragmented ones lose their identities farther downstream, presumably through viscous effects. This, therefore, would explain the increase in structure spacing with increasing $x$ since fewer structures survive with increasing $x$. These structures get energized by pairing or other means not understood yet, implying that some of the original structures never die. Therefore, new structures do not necessarily form as a result of local mean-flow instability. Our suggestion – which neither involves pairing nor instability – that some structures survive indefinitely while rearranging their spacing as other structures 'drop out', needs careful investigation, but appears consistent with the persistent effect of initial conditions in wakes (Wygnanski *et al.* 1986). Of course, in the case of a turbulent wake without any initially shed structure, say that of a porous plate, the instability of the local wake must produce the initial coherent structures (Castro 1971; Cimbala 1984; Wygnanski *et al.* 1986). We contend that such instability is neither of the mean profile, nor linear, nor of parallel flow. Increasing structure spacing with increasing $x$ has been reported by, among others, Taneda (1959), Gerrard (1966), Zdravkovich (1968), Matsui & Okude (1981) and Cimbala (1984).

### 3.3. *Detection based on structure centre*

By imposing a suitably selected threshold on the time-dependent smoothed vorticity signal, large-scale structures can be identified on the basis of vorticity concentration. However, as discussed in the previous section, there is large scatter between individual structure features. Therefore, the detection process must be preceded by the selection of the optimum transverse detection position $y_c$ at each measurement station. This selection was made from the histogram of structure centres detected as a function of $y$. The rake of X-wires was then shifted transversely so that it was centred at $y_c$. All data were then retaken. The histograms obtained after the relocation of the rake are shown in figure 3 only for structures of one sign, the number of passing structures being divided by the total number of initial, shed vortices. That is, $f$ is the structure passage frequency and $f_s$ is the shedding frequency. The detection condition used at this stage tentatively specified only the strength (denoted by the peak value of smoothed vorticity) and streamwise size of the structure. Figure 3 indicates broadening of the histogram with the streamwise distance, as to be expected from increasing transverse wandering of structures with increasing $x$. The line connecting the location of the peak of the histogram at each station can be considered as the most probable trajectory of shed vortices, and is shown as solid line in figure 3 denoting $y_c$ as a function of $x$. $y_c$ is about a half of the half-velocity-defect width $b$, denoted by a broken line in the figure. Thus, the streamwise variation of $y_c$ is nearly proportional to $x^{\frac{1}{2}}$ except in the vicinity of the cylinder.

### 3.4. *Detection criteria*

Since this work was an effort to develop a technique for eduction of coherent structures in a fully turbulent flow, the farthest downstream station, i.e. $x = 40d$, was chosen for development of the scheme. The dispersion in structure characteristics

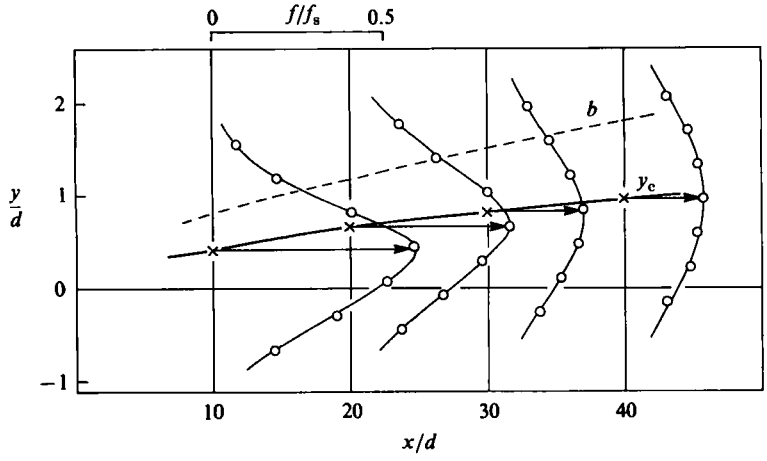


FIGURE 3. Structure passage frequency $f/f_s$.

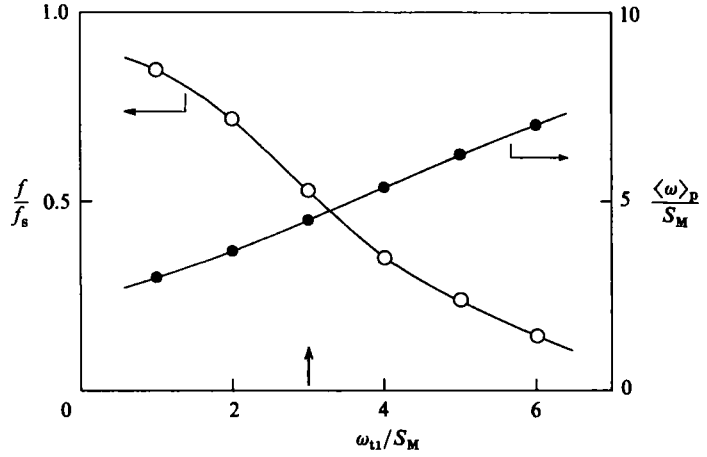


FIGURE 4. Number of accepted structure $f$ and peak coherent vorticity $\langle\omega\rangle_p$ as functions of threshold level ($x/d = 40$); ○, $f/f_s$; ●, $\langle\omega\rangle_p/S_M$.

being the largest at this station (figures 1 *d–g*), the eduction scheme should work better at the upstream stations. The present eduction scheme employs two principal conditions: one for the structure strength and the other for the structure size. We shall discuss these two first; further refinement of the eduction scheme will be discussed later.

As with any detection scheme, a structure was recognized by applying a threshold to the smoothed vorticity signal at the rake centre, i.e. $y = y_c$. Since structure strength (denoted by peak value of smoothed vorticity) is a local quantity, the local maximum mean shear $S_M$ appears to be the logical choice for specifying the threshold $\omega_{t1}$. In order to select the optimum threshold level, the number of structures detected at $y_c$ was determined as a function of the threshold $\omega_{t1}$. Figure 4 shows the number $f$ of detected structures per second and their ensemble-averaged peak vorticity $\langle\omega\rangle_p$ as a function of the threshold $\omega_{t1}$. With increasing $\omega_{t1}$, $f$ decreases monotonically and $\langle\omega\rangle_p$ increases almost linearly. The selection of the appropriate threshold level would

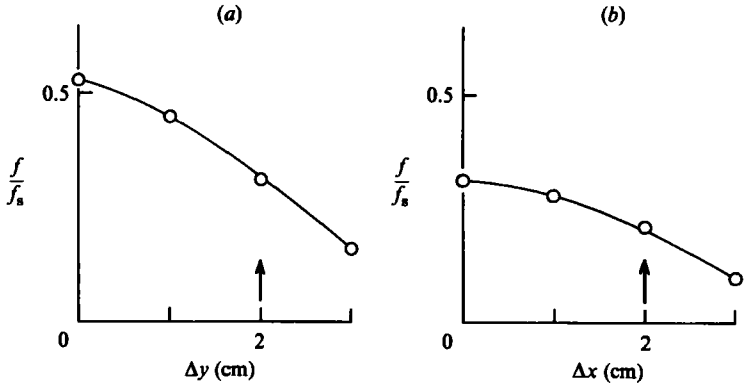


FIGURE 5. Number of accepted structures at $x/d = 40$; (*a*) transverse scale; (*b*) longitudinal scale, $\Delta x = U_c \Delta t$.

be straightforward if these variations had a plateau with respect to $\omega_{t1}$: the midpoint of the plateau region would be the most suitable choice for $\omega_{t1}$. In reality, however, such a plateau seldom exists in a fully turbulent environment as the structure measures typically have a monotonic variation with respect to the threshold level. This is where the judgement (hence prejudice!) of the experimentalist is critical. It is somewhat subjective to select the most preferable value from figure 4; the threshold level $\omega_{t1}$ was chosen as $3S_M$ (figure 4); at $x/d = 40$, this results in the detection of about half of the shed vortices. After detecting structures with peak vorticity values higher than $\omega_{t1}$, the locations of the structure centres corresponding to the peak vorticity are assigned the coordinates $(y_c, t_c)$, and the reference time instant $t_c$ is stored in a computer file.

The next step is to specify the size of the underlying structure. That is, the instantaneous vorticity should be well correlated over a certain distance around each structure centre $(y_c, t_c)$. For convenience, and to reduce computer time for data analysis, we require instantaneous coherence of vorticity only in streamwise and transverse directions around the centre and not over an area around the centre. The transverse size is evaluated from (smoothed) vorticity values at various transverse distances $\Delta y$ on both sides of $y_c$ at the time instant $t_c$; that is, by playing back the data tape, we single out vorticity signals only at the previously determined reference time instant $t_c$ and compare $\omega(y_c \pm \Delta y, t_c)$ with the centre value $\omega(y_c, t_c)$. The criterion chosen is that the vorticities at $(y_c \pm \Delta y, t_c)$ must have the same sign as that at the centre and must have values higher than a threshold $\omega_{t2}$ but lower than the centre value (which, of course, must simultaneously be higher than $3S_M$). That is, the joint condition must be satisfied simultaneously at these three $y$-locations. This condition assures that the accepted structures are centred at $y_c$ and thus rejects transversely shifted structures. After some iterative explorations, we chose the threshold as $\omega_{t2} = 0.5S_M$, and the population of structures satisfying this condition was determined as a function of $\Delta y$ (figure 5*a*). There is no clear guidance for the choice of $\Delta y$: too small a value will result in the selection of disparate structures, and too large a value will result in the selection of very few structures. Based on the data in figure 5(*a*), we chose $\Delta y$ to be 2 cm, which is about $0.4b$ at $x/d = 40$.

Virtually the same criterion was applied for the streamwise size of the structure. We assume short-time validity of Taylor's hypothesis; that is, the streamwise scale $\Delta x$ can be approximated by $U_c \Delta t$. Then we impose the condition that the smoothed

vorticities at $(y_c, x_c \pm U_c \Delta t)$ must be of the same sign as that at the centre and must be higher than $0.5S_M$, while the value at the centre $(y_c, t_c)$ is higher than $3S_M$. Thus, the number of structures accepted by this additional criterion decreases further (figure 5*b*), as to be expected. After examining the sensitivity of the shape of the educed structure to the choice of $\Delta x$, we selected $\Delta x \approx \Delta y$ (exactly the same value cannot be chosen because $\Delta y$ and $\Delta t$ are discrete variables). This choice seems satisfactory because we do not expect the cross-section of the dominant structure to be highly elongated. In this sense the criteria for the structure size implicitly include a mild condition for the structure shape also. However, the size criteria are chosen sufficiently conservatively that a variety of sectional shapes will still survive through the eduction scheme, and the eduction will retain the dominant structure shape – circular or not.

We imposed the transverse size condition only at the time instant $t_c$. A better, but time consuming, alternative may be to take short-time cross-correlation between smoothed vorticity signals on both sides of $y_c$ and require that these two signals be well correlated; this condition has been used in our laboratory by Tso (1983) for eduction (as well as selection of structure modes) in the far field of a turbulent circular jet.

### 3.5. *Conditional average and enhancement*

Large-scale structures will be accepted only when all the criteria mentioned above are satisfied so that weaker, smaller, fragmented, distorted or transversely shifted advecting structures will be discarded from the ensemble average. With the structure centre as a phase (i.e. time) reference, signal segments around accepted structures are relatively aligned with respect to their centres $(y_c, t_c)$, i.e. their reference points, and then ensemble-averaged. This is the *zeroth-iteration ensemble average*.

Since smoothed vorticity peaks may not be sharp or may not be clearly identified, it is necessary to refine further the alignment process outlined above in an attempt to sharpen the educed structure details and minimize the jittering effect of structure property dispersion. This is achieved by taking the cross-correlation of individual structure vorticity and the zeroth-iteration ensemble-average vorticity (both as functions of time through structure centre). The signal length for the correlation calculation was chosen to be $0.8T_s$, i.e. $0.4T_s$ on either side of each centre $t_c$. Each realization is then relatively re-aligned (i.e. $t_c$ is shifted) by the time shift $\tau$ which equals the time delay of the peak correlation from zero time. In practice, instead of shifting the signal of each realization, the original $t_c$ value stored in the data file was revised, by changing it by the time shift $\tau$. This type of time alignment has been employed in the eduction of spark-induced turbulent 'spots' in turbulent environments (Zilberman *et al.* 1977; Kleis *et al.* 1981). In those studies, time-alignment was determined by correlating longitudinal velocity signals only. For the zeroth-iteration, the reference times in the signal traces were inferred from the time elapsed from the initiation of the spot, namely the spark that induces the 'spot'. In the present case, the structure arrival time is neither known nor necessary, since the structure alignment is based on the measured, local smoothed vorticity signal itself.

The cross-correlation as a function of time shift was calculated not at various transverse locations but only at the centre section of the structure (i.e. at $y = y_c$), and the structures were then further re-aligned by time-shifting $t_c$ by the time delay of peak correlation of individual structure vorticity with the zeroth-iteration ensemble-average vorticity. The ensemble average of these aligned structures is the *first-iteration ensemble average*. This alignment can be iterated upon until convergence (in contour shape and peak values of vorticity) is achieved. However, in the present

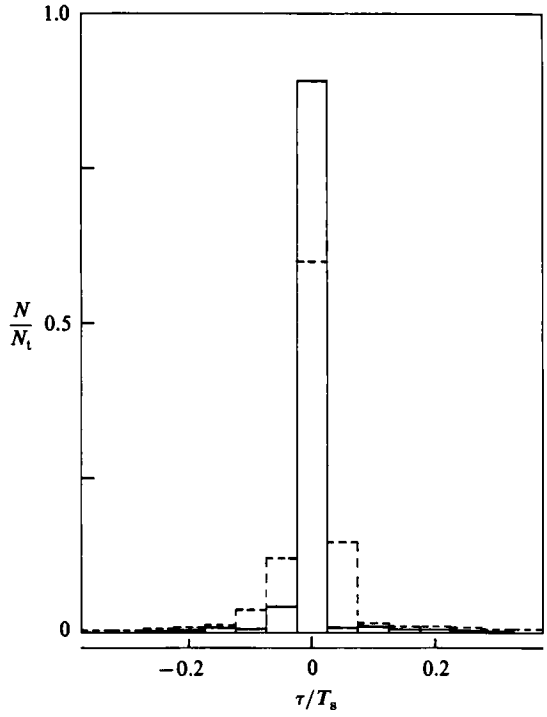


FIGURE 6. Histogram of accepted structures during alignment process; ——, after alignment; – – – –, before alignment.

case only one iteration step in alignment gave a satisfactory result. Figure 6 shows an example at $x = 40d$ of the histogram of time shift $\tau$ before and after alignment by the first iteration. In the zeroth-iteration ensemble average, 60% of total structures do not require any further alignment, as seen in the figure. That is, the identification of the peak in a smoothed vorticity contour itself aligns satisfactorily 60% of all structures centred at $y_c$. This percentage increases at the farther-upstream stations (for example, 70% at $x = 20d$). At $x = 40d$, 90% of the total accepted structures are already aligned after the first iteration. We discarded the remaining 10% that are not yet aligned because the accepted structures were already adequate in number (typically a few hundred), and especially because those structures requiring excessive time shifts for alignment must have abnormal features and can be regarded as 'freak'.

So far, the rejection is based on shifts required for time-alignment. As a next step in the improvement of eduction, further rejection was carried out by discarding structures with weaker identity. That is, a realization was discarded if the peak value of the correlation of its vorticity with the iterated ensemble-averaged vorticity was lower than a specified level $R_t$; this level was chosen as

$$R_t = \frac{1}{2N} \sum_{i=1}^{N} R_i$$

($R_i$ is the peak correlation value for the $i$th realization, and $N$ is the total number of realizations retained up to this stage). That is, realizations that show weak resemblence (indicated by low values of peak correlation) to the ensemble average

are also rejected. This enhancement procedure was adopted in order to sharpen further the educed structure features.

The initial centre $t_c$ of each structure was revised by the cumulative time shifts determined successively from iterative cross-correlations discussed above, and the corresponding finally revised point $t_c$ on the vorticity map denotes the true centre of the (underlying) coherent structure. Various quantities in the signal around the times $t_c$ are then ensemble averaged. Note that we use the smoothed vorticity to determine time shifts required for optimum alignment of the underlying organized structures before ensemble-averaging and also to determine which structures are to be discarded from the ensemble average on the basis of structure identity. Once the structures that need to be retained are identified and the corresponding necessary time shifts known, the smoothing process has served its purpose and the *smoothed* signals are then discarded; only *unsmoothed* (raw) signals centred around the revised values of $t_c$ are then used for ensemble averaging in order to educe the structure. In this study, the number of structures accepted in the final ensemble average was about 700 (note that this amounts to 13% in table 1).

It may be necessary to re-emphasize that such an elaborate eduction scheme as adopted in this study does not create an artificial structure, but merely helps select the dominant natural structure (preferred mode) and sharpen the educed structure details. Without a rigorous scheme like this, the educed structure will be excessively smeared and will reveal very little instantaneous flow physics.

To summarize, the present eduction process consists of the following steps: (i) determine the most probable transverse location $y_c$ of vortex centres, (ii) position the sensor array by centring it at $y_c$, (iii) obtain instantaneous smoothed spanwise vorticity, (iv) consider only vorticity concentrations that are centred at $y_c$, (v) select a threshold value $\omega_{t1}$ for the peak (smoothed) vorticity on the basis of the local flow characteristics (here $\omega_{t1} = 3S_M$), (vi) identify the instants $t_c$ of the apparent centres of structures by requiring the smoothed vorticity at $y_c$ to be transversely maximum at $t_c$ and to be higher than the threshold $\omega_{t1}$, (vii) specify the structure size ($\Delta x \approx \Delta y$) to be comparable to $nb$ (here $n = 0.4$) in both transverse and streamwise directions, by requiring that smoothed vorticity at $(t_c \pm \Delta x/U_c)$ and at $(y_c \pm \Delta y)$ are of the same sign as $(t_c, y_c)$ and higher than a threshold $\omega_{t2}$ which may be expressed in terms of $\omega_{t1}$ (here $\omega_{t2} = \omega_{t1}/6$), (viii) iteratively determine the true structure centre by determining the time-shifts necessary for maximum cross-correlation between each structure vorticity and ensemble-average vorticity, (ix) discard structures requiring excessive time shifts, (x) discard structures with insufficient identity, i.e. those producing low peak correlation with the ensemble average, (xi) align segments of unsmoothed (raw) signals with respect to the refined structure centres $(y_c, t_c)$ determined from cumulative time shifts, and (xii) perform appropriate ensemble averaging to educe coherent structure and incoherent turbulence properties.

The coherent-structure eduction after alignment involves computations of coherent and incoherent components $\langle f \rangle$ and $f_r$ of any signal $f$. That is

$$f(\boldsymbol{x}, t) = \langle f(\boldsymbol{x}, t) \rangle + f_r(\boldsymbol{x}, t),$$

where

$$\langle f(\boldsymbol{x}, t) \rangle = \frac{1}{N} \sum_{i=1}^{N} f(\boldsymbol{x}, t_{ci} + t),$$

and $t_{ci}$ corresponds to the location in time of the centre of the $i$th structure. In other words, whatever survives the ensemble averaging of finally aligned *unsmoothed*

| Criterion | $f/f_s(\%)$ | $\langle\omega\rangle_p/S_M$ |
|---|---|---|
| 1. $\omega_p > \omega_{th}$ | 53 | 4.5 |
| 2. Size in $y$ | 31 | 5.1 |
| 3. Size in $x$ | 21 | 5.3 |
| 4. Alignment | — | 5.4 |
| 5. $R_{\omega_p\omega} > R_{th}$ | 13 | 5.7 |

TABLE 1. Number of accepted structures and peak vorticity at each step of the eduction process

signals is the coherent structure $\langle f\rangle$. The departure of each unsmoothed realization from the ensemble average $\langle f\rangle$ is the corresponding incoherent turbulence $f_r$.

From the aligned unsmoothed signal traces $u(y,t)$, $v(y,t)$, ensemble averaging results in coherent longitudinal and lateral velocities $\langle u\rangle$ and $\langle v\rangle$. The departure of unsmoothed signals $(u,v)$ from $(\langle u_c\rangle, \langle v_c\rangle)$ gives the corresponding incoherent turbulence traces $(u_r, v_r)$. For convenience, the following notation is used $u_c = \langle u\rangle - U_c, v_c = \langle v\rangle$, where $U_c$ is the streamwise advection velocity of the structure. Thus, $u_c$ is the coherent longitudinal velocity in the frame fixed to the structure centre. The following quantities are then computed:

$$\langle u(y,t)\rangle = \frac{1}{N}\sum_{i=1}^{N} u(y, t_{ci}+t),$$

$$\langle v(y,t)\rangle = \frac{1}{N}\sum_{i=1}^{N} v(y, t_{ci}+t),$$

$$u_r(y,t) = u(y,t) - \langle u(y,t)\rangle, \quad v_r(y,t) = v(y,t) - \langle v(y,t)\rangle,$$

$$\langle u_r^2\rangle^{\frac{1}{2}}(y,t) = \left\{\frac{1}{N}\sum_{i=1}^{N} u_r^2(y,t)\right\}^{\frac{1}{2}},$$

coherent vorticity,

$$\langle\omega\rangle = \frac{\partial v_c}{\partial x} - \frac{\partial u_c}{\partial y}.$$

As an example, the number of accepted structures and the corresponding peak coherent vorticity value at each step of the eduction process at the station $x = 40d$ are listed in table 1.

## 4. Transient behaviour of structure

### 4.1. *Coherent vorticity*

Ensemble-averaged spanwise vorticity contours at the four $x$-stations (i.e. $x/d = 10$, 20, 30 and 40) are shown in figures 7(*a–d*). The flow direction is from left to right. The detected and aligned structure (i.e. below the centreline) is represented by solid lines and the opposite-signed vorticity contours denoting structures shed from the top side of the cylinder are shown by broken lines. Coordinates are appropriately normalized by the advection velocity $U_c$ and the cylinder diameter $d$ for convenience of direct comparison at all $x$. The coherent vorticity contour shape does not change between $x$ and $t$ coordinates because of the use of a constant advection velocity $U_c$ (over the structure extent) in Taylor's hypothesis invoked in the eduction process.

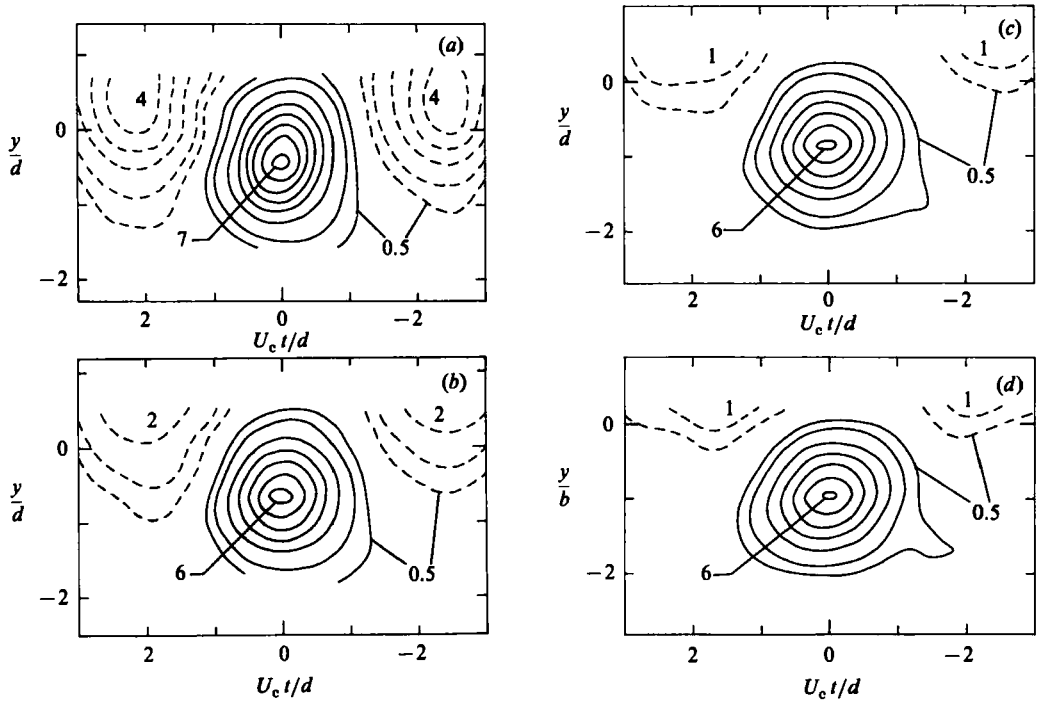


FIGURE 7. Coherent vorticity contours $\langle\omega\rangle/S_M$ at: (*a*) $x/d = 10$; (*b*) 20; (*c*) 30; (*d*) 40; contour levels: 7, 6, 5, 4, 3, 2, 1, 0.5.

Also, structure evolution is gradual in a wake. Thus, figure 7 denotes essentially the spatial structure patterns.

As was also evident in figure 1, the educed structure does not grow substantially in size with increasing $x$; rather, when the size is identified by the same relative contour level, the structure remains almost constant in size, and thus the size relative to the wake width decreases downstream. The shape of the structure, which is initially somewhat elongated in the transverse direction, becomes rounded with increasing $x$, while the orientation progressively becomes inclined and aligned with the direction opposed to the mean shear. Such an inclination, which is contrary to one's intuition, is associated with co-gradient production; if the inclination is aligned with the mean shear direction, production should be of the counter-gradient type (Browand 1980; Hussain 1983*a*). This preferred orientation of the educed structure cannot be an artifact of the eduction scheme, but is real, because the detection conditions on the local flow variables even assume a nominal symmetry with respect to the structure centre. The values of structure spacing ratio (i.e. transverse-to-longitudinal separation ratio) of the educed structures at $x/d = 10$, 20, 30, 40 are roughly 0.20, 0.30, 0.37, 0.43, respectively, in contrast with the theoretical value of 0.281 for the Kármán vortex street.

The alternating structures lose their regularity in shape, size, strength and spacing with increasing $x$. Smearing increases with increasing distance from the detection or *alignment point* (i.e. $t = 0$); the decrease of contour-level values of (broken-lined) structures relative to the aligned (solid-lined) structure reflects the degree of jitter (of the two structures on either side of the figures 7*a–d*) relative to the alignment point. Both the contour-level value and identity of dashed contours show large

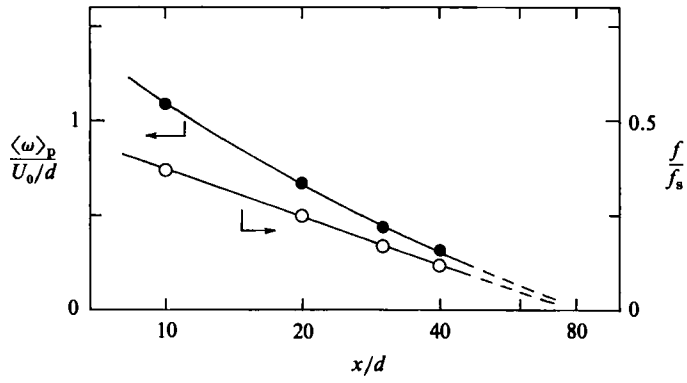


FIGURE 8. Streamwise variation of the peak coherent vorticity $\langle\omega\rangle_p$ and the accepted number $f$ of structures; ●: peak vorticity; ○: accepted number.

| $x/d$ | 5.4† | 10 | 20 | 30 | 40 |
|---|---|---|---|---|---|
| $\langle\omega\rangle d/U_0$ | 1.33 | 1.09 | 0.67 | 0.44 | 0.32 |
| $\langle\omega\rangle/S_M$ | — | 7.2 | 6.4 | 6.2 | 6.1 |
| $u_c/U_0$ | (+0.18‡ | +0.22 | +0.16 | +0.12 | +0.09 |
| | (−0.17) | −0.22 | −0.15 | −0.11 | −0.09 |
| $v_c/U_0$ | (+0.49) | +0.30 | +0.17 | +0.10 | +0.07 |
| | (−0.35) | −0.27 | −0.14 | −0.08 | −0.06 |
| $\langle u_r'\rangle/U_0$ | (0.28) | 0.17 | 0.12 | 0.09 | 0.07 |
| $\langle v_r'\rangle/U_0$ | (0.30) | 0.16 | 0.11 | 0.08 | 0.07 |
| $-u_c v_c/U_0^2$ | (+0.029) | +0.031 | +0.015 | +0.007 | +0.004 |
| | (−0.021) | −0.039 | −0.014 | −0.006 | −0.003 |
| $\langle -u_r v_r\rangle/U_0^2$ | (0.019) | 0.013 | 0.006 | 0.003 | 0.002 |
| $2\langle S\rangle/S_M$ | — | 3.4 | 2.7 | 2.2 | 2.3 |
| $\langle P\rangle d/U_0^3$ | (0.012) | 0.0049 | 0.0013 | 0.0004 | 0.0002 |
| $\langle P\rangle/U_0^2 S_M$ | — | 0.0324 | 0.0124 | 0.0044 | 0.0030 |
| $\langle P_s\rangle/U_0^2 S_M$ | — | 0.0314 | 0.0123 | 0.0044 | 0.0028 |
| $\langle P_n\rangle/U_0^2 S_M$ | — | 0.0096 | 0.0031 | 0.0012 | 0.0010 |
| $\langle P_s\rangle/\langle P_n\rangle$ | — | 3.3 | 4.0 | 3.7 | 2.8 |
| $U_C/U_0$ | 0.83 | 0.87 | 0.875 | 0.885 | 0.89 |

† After Cantwell & Coles (1983)
‡ values at the maximum contour level

TABLE 2. Peak values of ensemble-averaged properties

increases in smearing with increasing $x$. The tongue projecting to the right of the aligned structure is real but its significance is unclear. The streamwise variation of the peak coherent vorticity (non-dimensionalized by free-stream velocity $U_0$ and $d$) and the accepted structure number are plotted in figure 8. Extrapolation of these curves suggests that the shed vortices eventually disappear at around $80d$. However, this does not necessarily imply complete decay of coherent structures. Distortion, including evolution of strong three-dimensionality and partial tearing (and even partial pairing), presumably occurs, resulting in loss of the identity of primary vortices (also inferred from the instantaneous vorticity maps in figure 1). Cimbala (1984) observed that the location of disappearance of primary vortices moved upstream with increasing Reynolds number, and he did not see residual vortices

beyond $x = 50d$ for $Re_d > 160$. This relatively earlier decay of the primary vortices compared to our data (i.e. figure 8) seems to indicate the limitation of visual observation in accurately recognizing lower-wavenumber structures in the fully turbulent field. This also underlines the critical need for direct structure measurements like the ones presented here. Note that while the number and the absolute peak vorticity value of strong structures decrease with increasing $x$ (see figure 8), the structure strength relative to the local maximum mean strain rate $S_M$ remains in apparent equilibrium at a value of about 6, but the structure size relative to the local wake width decreases (figures 7*a–d*). This is in contrast with the case of a plane mixing layer in which large-scale structures evolve into an equilibrium state in size and strength (Hussain & Zaman 1982; Metcalfe *et al.* 1986).

### 4.2. *Other structure measures*

In this subsection, the ensemble-averaged flow properties are briefly discussed with emphasis on their streamwise evolution. The detailed flow physics will be discussed in the next section

The experimentally determined peak values of various quantities at each $x$-station are listed in table 2. The table includes CC's data for a structure centred at $x/d = 5.44$ and $y/d = 0.22$ (their phase 7). Note that direct comparison of our data with theirs is not totally meaningful because the absolute values must differ owing to the use of different eduction techniques. Here, the following definitions are used on the basis of double decomposition (see Hussain 1983*a*):

coherent velocities: $u_c = \langle u \rangle - U_c, \quad v_c = \langle v \rangle,$

incoherent turbulence intensities: $\langle u_r' \rangle = \langle u_r^2 \rangle^{\frac{1}{2}}, \quad \langle v_r' \rangle = \langle v_r^2 \rangle^{\frac{1}{2}},$

Reynolds stress: coherent part $= -u_c v_c$, incoherent part $= -\langle u_r v_r \rangle,$

coherent strain rate: $\langle S \rangle = \frac{1}{2}\left(\frac{\partial \langle u \rangle}{\partial y} + \frac{\partial \langle v \rangle}{\partial x}\right),$

coherent production: $\langle P \rangle = \langle P_s \rangle + \langle P_n \rangle,$

coherent shear production: $\langle P_s \rangle = \langle -u_r v_r \rangle \left(\frac{\partial \langle u \rangle}{\partial y} + \frac{\partial \langle v \rangle}{\partial x}\right),$

coherent normal production: $\langle P_n \rangle = -\langle u_r^2 \rangle \frac{\partial \langle u \rangle}{\partial x} - \langle v_r^2 \rangle \frac{\partial \langle v \rangle}{\partial y}.$

All quantities are non-dimensionalized by $U_0$ and $d$. Note that the values of CC cited are their maximum contour levels.

Contour plots of typical structure measures at the two extreme stations (i.e. at $x = 10d$ and $40d$) are compared in figures 9(*a–j*); these are $u_c$, $v_c$, $\langle q_r^2 \rangle = \langle u_r^2 \rangle + \langle v_r^2 \rangle$, $-\langle u_r v_r \rangle$ and $\langle P \rangle$. Data at intermediate stations have intermediate shapes and values and are thus not shown for space conservation. In each figure, the structure centre inferred from the peak coherent vorticity (figure 7) is denoted by the + mark, and the structure boundary is denoted by dotted lines; these two constitute the common reference between various figures. The structure boundary chosen is that with the vorticity contour level of $\langle \omega \rangle / S_M = 1$ in figure 7.

The velocity components clearly show the rotational motion associated with the structure (figures 9*a–d*). At each station, the absolute values of positive and negative peaks of $u_c$ are about the same, while the negative peak of $v_c$ (outward flow) is always

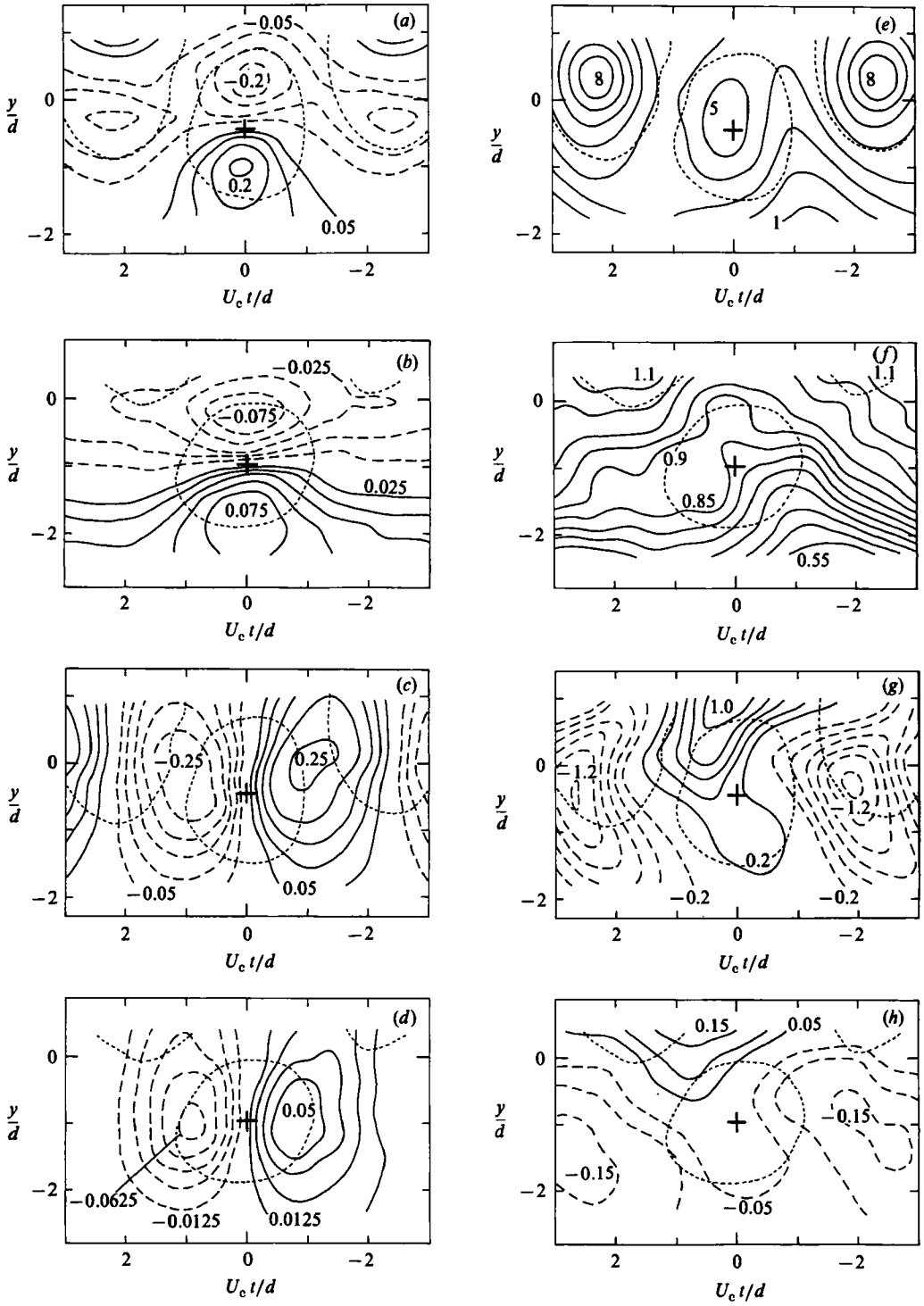


FIGURE 9(a–h). For caption see facing page.

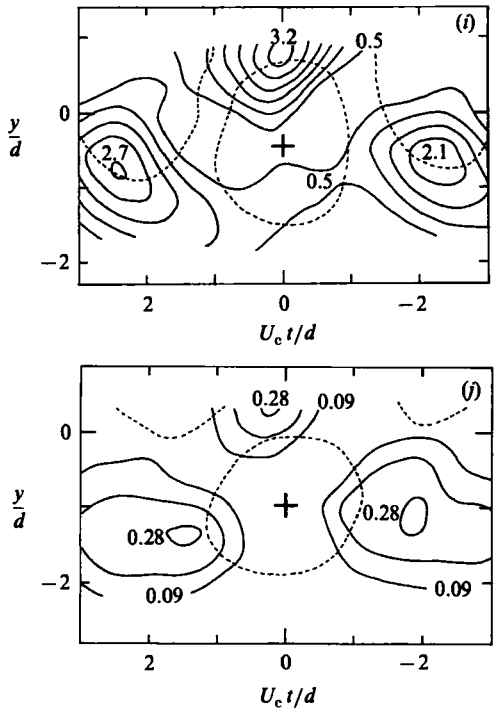


FIGURE 9. Comparison of structure properties at $x/d = 10$ and 40. (*a*) $u_c/U_0$ at $x/d = 10$, levels: $\pm 0.2$, $\pm 0.15$, $\pm 0.1$, $\pm 0.05$; (*b*) $u_c/U_0$ at $x/d = 40$, levels $\pm 0.075$, $\pm 0.0625$, $\pm 0.05$, $\pm 0.0375$, $\pm 0.025$; (*c*) $v_c/U_0$ at $x/d = 10$, levels: $\pm 0.25$, $\pm 0.2$, $\pm 0.15$, $\pm 0.1$, $\pm 0.05$; (*d*) $v_c/U_0$ at $x/d = 40$, levels: $\pm 0.0625$, $\pm 0.05$, $\pm 0.0375$, $\pm 0.025$, $\pm 0.0125$; (*e*) $\langle q_r^2 \rangle / U_0^2$ at $x/d = 10$, levels: 8, 7, 6, 5, 4, 3, 2, 1 ($\times 10^{-2}$); (*f*) $\langle q_r^2 \rangle / U_0^2$ at $x/d = 40$, levels: 1.1, 1.05, 1.0, 0.95, 0.9, 0.85, 0.8, 0.75, 0.7, 0.65, 0.6, 0.55 ($\times 10^{-2}$); (*g*) $\langle -u_r v_r \rangle / U_0^2$ at $x/d = 10$, levels: $\pm 1.2$, $\pm 1.0$, $\pm 0.8$, $\pm 0.6$, $\pm 0.4$, $\pm 0.2$ ($\times 10^{-2}$); (*h*) $\langle -u_r v_r \rangle / U_0^2$ at $x/d = 40$, levels: $\pm 0.15$, $\pm 0.1$, $\pm 0.05$ ($\times 10^{-2}$); (*i*) $\langle P \rangle / (U_0^2 S_M)$ at $x/d = 10$, levels: 3.2, 2.7, 2.1, 1.6, 1.1, 0.5 ($\times 10^{-2}$); (*j*), $\langle P \rangle / (U_0^2 S_M)$ at $x/d = 40$, levels: 0.28, 0.18, 0.09 ($\times 10^{-2}$).

slightly larger than the positive peak (inward flow). The larger negative peak value of $v_c$ is consistent with the gradual motion of structures away from the wake centreline. Furthermore, the maximum of $v_c$, which is initially higher than that of $u_c$ (figures 9*a*, *c*), decreases relatively faster and becomes lower than the $u_c$ peak value beyond $x = 30d$ (figures 9*b*, *d*). The up–down anti-symmetry of the $u_c$ contours is consistent with the fact that the structure advection velocity $U_c$ in the streamwise direction has been subtracted out to obtain $u_c$; $v_c$ is supposed to be asymmetric in $t$ because the transverse structure celerity $V_c$, though small, has not been subtracted out to obtain $v_c$.

As regards the velocity field, a comment should be made about the structure advection velocity $U_c$. By definition, $u_c$ is necessarily zero at the structure centre. Therefore, the advection velocity used can be checked from the ensemble-averaged velocity $\langle u \rangle$ at the structure centre. Values of $U_c$ determined from $\langle u \rangle$-contours at the location of the structure centre (identified by peak vorticity) are $0.87U_0$, $0.875U_0$, $0.885U_0$ and $0.89U_0$ at the four measurement stations and are listed in table 2. The corresponding mean velocities at the detection position $y_c$ are $U/U_0 = 0.85$, 0.86, 0.875 and 0.89. The agreement between the two sets of values is close; the maximum

difference is $0.02U_0$ and occurs at $x = 10d$. Considering the fact that a finite ensemble size is used to obtain $\langle u \rangle$-contours, the agreement is surprisingly good, and confirms the adequacy of the ensemble size accepted in the eduction scheme. These data trends, when extrapolated upstream, are consistent with the near-wake data of CC. The present calculation has ignored the transverse structure celerity $V_c$. Rough estimation of this value is possible from the average trajectory of the structure centre (figure 3); the estimated values of $V_c$ at $x = 20d$ and $30d$ are $0.016U_0$ and $0.013U_0$ respectively, which are much smaller than CC's value of $0.057U_0$ at $x = 6.5d$.

The total incoherent turbulence intensity $\langle q_r^2 \rangle / U_0^2$ (excluding the spanwise component $\langle w_r' \rangle$, which was not measured but is likely to be comparable to $\langle u_r' \rangle$ or $\langle v_r' \rangle$), has its maximum at almost the structure centre at $x = 10d$ (figure 9*e*). However, this maximum is obscured downstream (see figure 9*f* for $x = 40d$). This is not surprising considering the low values of $\langle u_r' \rangle$ or $\langle v_r' \rangle$ (being about $0.07U_0$) at $x/d = 40$. Perhaps a more rigorous detection scheme, including a three-dimensional array of vorticity sensors would educe sharper contours of $\langle q_r^2 \rangle$ at the larger downstream locations. Based on our studies of coherent structures in other flow geometries (Hussain 1981*a*, 1983*a*, *b*), we expect the $\langle q_r^2 \rangle$-contours to peak at around the structure centre.

Turbulence intensities decrease at a relatively slower rate than $(u_c, v_c)$ and become comparable to the absolute peak values of $u_c$ and $v_c$ at the last station (table 2). The particularly high value of $v_c$ in the near field is a peculiar feature of the wake. The data of CC showed that the $v_c$ peak at $x = 3d$ is about $0.6U_0$, being much larger than the $u_c$ peak value of $0.25U_0$. These high values are reasons why stationary hot wires cannot be used in the region close to a cylinder.

As shown in figures 9(*g*, *h*), the incoherent Reynolds stress always has a lower value around the structure centre and a maximum at the edge of the structure. Turbulence production (figures 9*i*, *j*) by the large-scale structure occurs mostly at about the same location as the $\langle -u_r v_r \rangle$-peaks. The contour patterns of both quantities are essentially similar at all $x$-stations. The contours of Reynolds stress and production will be discussed further in the next section.

## 5. Dynamics of coherent structure

### 5.1. *Details of coherent structure properties*

The data discussed so far have emphasized the characteristics of the flow field on one side of the wake centreline. A complete data set was retaken at one station only (i.e. $x = 20d$) with the hot-wire rake spanning the wake equally across the centreline; in this section, these data are discussed. Since the most interesting and important aspect of coherent structures are their topological features (Coles 1983; Hussain 1981*a*), the following discussions address these features (see also Perry & Watmuff 1981; Perry, Chong & Lim 1982; CC).

The unique feature in the near wake is the presence of alternating, counter-rotating, predominantly spanwise vortices. Topologically, the flow pattern is characterized by two critical points: one is the 'centre' specified by the location of peak coherent spanwise vorticity and the other is the 'saddle' located between structures and characterized by a minimax of coherent spanwise vorticity. Hussain (1981*a*, *b*) reported the spatial distribution of coherent production data and emphasized the role of the saddle in turbulence production in a mixing layer. Later, CC suggested that the dominant topological feature of the near wake is the formation and evolution of the saddle region and explained the structure dynamics by focusing on the role of

the saddle. Indeed, our wake results also support this point of view, particularly the significance of the saddle region in turbulence production. Our data appear to be advantageous in discussing the detailed topological features because the detection and eduction procedure guarantees all quantities to have been adequately educed (by proper alignment) with respect to the structure centre; these quantities are likely to be smeared significantly in an eduction triggered not locally but by an upstream reference event.

To start the discussion, various ensemble-averaged quantities are shown in figures 10(*a–k*) for an intermediate station, namely $x/d = 20$, where the flow is fully turbulent, yet the structure signature is sufficiently strong. These include: (*a*) velocity-vector pattern relative to the frame frozen with the structure, i.e. advected with a velocity $U_c$; (*b*) coherent vorticity; (*c*, *d*) coherent velocity components; (*e*) incoherent turbulence intensity; (*f*) incoherent Reynolds stress; (*g*) coherent Reynolds stress; (*h*) coherent strain rate; and (*i–k*) coherent production. The centre (marked by +) and the boundary of the structure (vorticity level $\langle\omega\rangle/S_M = 1$) together with the saddle point (marked by ×) are shown in all the figures. The coordinates are non-dimensionalized by the half width $b$ and the structure advection velocity $U_c$, while the quantities are appropriately non-dimensionalized by the free-stream velocity $U_0$.

As expected, the velocity-vector pattern (figure 10*a*) clearly shows rotational fluid motion around the centre (+ mark), and also specifies the location of the saddle point (× mark). The coherent vorticity field definitely shows well-organized large-scale vorticity concentrations about the wake centreline (figure 10*b*). The two vortices (A and C) away from the aligned vortex (B) have lower peak vorticity because of the unavoidable jitter away from the trigger point. Note that velocity vectors around the aligned structure B centred at the alignment point $t = 0$ are much longer than those around A or C. There should be little doubt that the true contours of A and C will be identical with that of B, but inverted about the wake centreline. However, the small differences in the contour shapes are within the experimental uncertainty of the technique and are of no significance in the context of this discussion. The large difference in peak vorticity values between structures A (or C) and B is indicative of the extent of jitter caused by unequal spacing, strength and transverse displacement of adjacent structures. Note that $u_c$ (figure 10*c*) is not the deviation from the time-averaged velocity but is the total phase-average longitudinal velocity in a frame advected with the structure, i.e. $u_c = \langle u\rangle - U_c$. The maximum contour level of $u_c$ corresponds to $\langle u\rangle/U_0 = 1.15$, a value even higher than the free-stream velocity. This is not unexpected as the free-stream fluid must be accelerated while moving past the large-scale structure. Viewed another way, $\langle u\rangle$ at the edge of the wake consists of contributions from both the free-stream velocity and the velocity induced by the coherent structures. The zero value of $u_c$ at the structure centre confirms the accuracy of the $U_c$ value.

The $v$-component has an almost symmetric distribution in $x$ with respect to the centre (figure 10*d*). The inward velocity along the front (downstream side) of the structure is due to structure rotation minus the contribution due to the (gradual) structure movement away from the centreline, while the outward motion at the back (upstream side) is contributed by both structure rotation and outward structure movement. Note that the contour pattern of $v_c$ is a superposition of two adjacent structures across the centreline, i.e. motions associated with two structures from two sides of the wake centreline. That is, the inward motion in the front of an educed structure B, for example, is also partially contributed to by the outward motion at

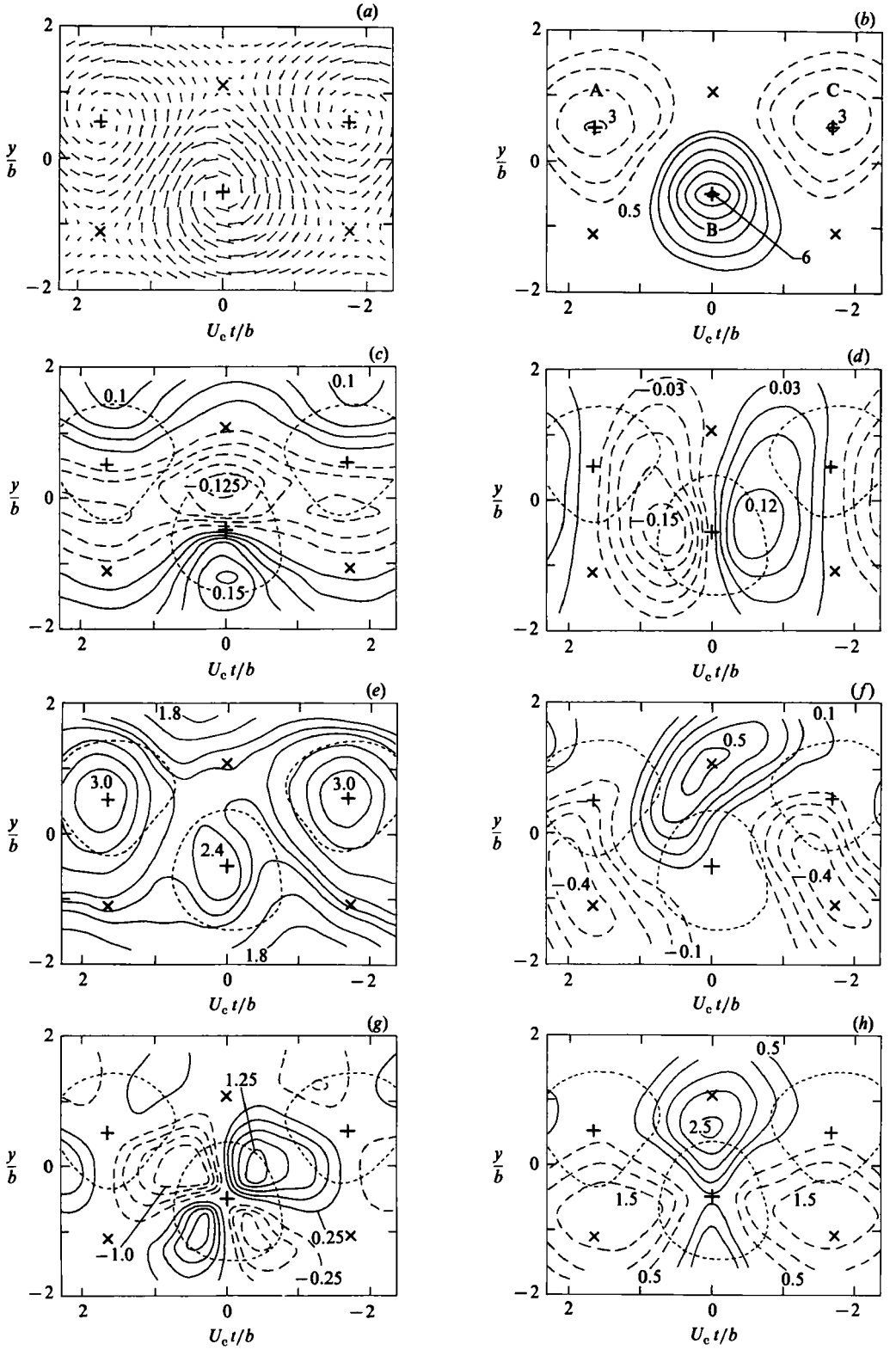


FIGURE 10(*a–h*). For caption see facing page.

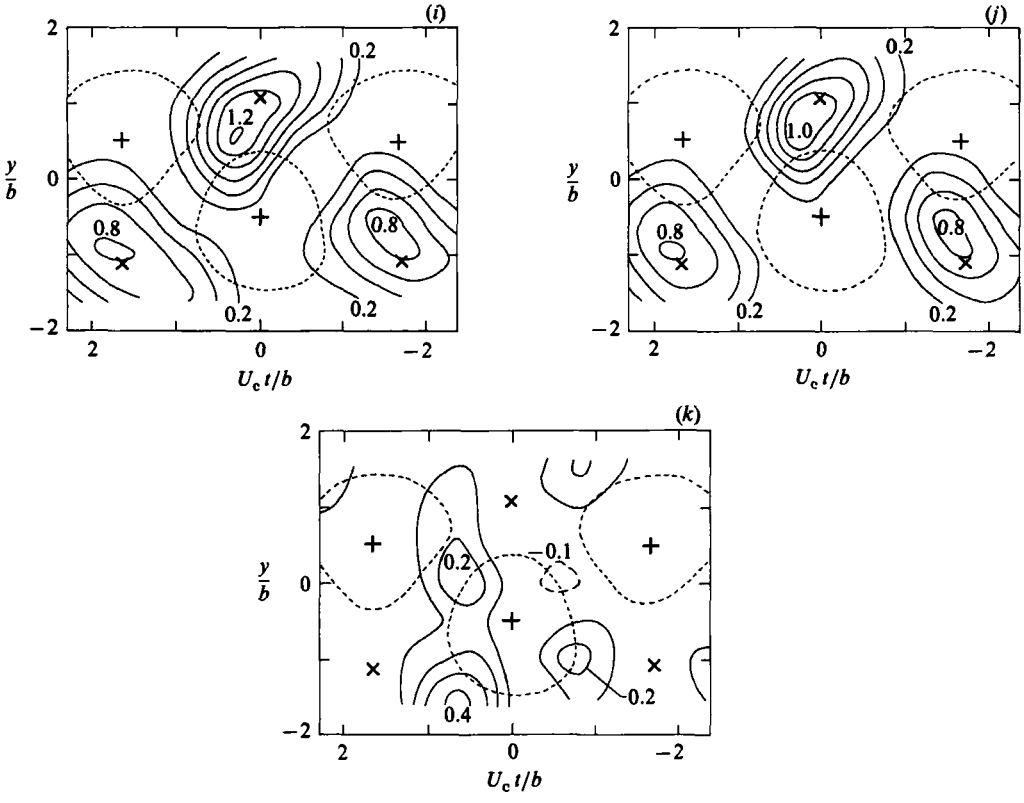


FIGURE 10. Structure properties at $x/d = 20$. (*a*) velocity-vector pattern; (*b*) coherent vorticity $\langle\omega\rangle/S_m$; levels: 6, 5, 4, 3, 2, 1, 0.5; (*c*) coherent longitudinal velocity $u_c/U_0$; levels: $\pm0.15$, $\pm0.125$, $\pm0.1$, $\pm0.075$, $\pm0.05$, $\pm0.025$; (*d*) coherent transverse velocity $v_c/U_0$; levels: $\pm0.15$, $\pm0.12$, $\pm0.09$, $\pm0.06$, $\pm0.03$; (*e*) incoherent turbulence energy $\langle q_r^2\rangle/U_0^2$; $q_r^2 = u_r^2 + v_r^2$; levels: 3.0, 2.8, 2.6, 2.4, 2.2, 2.0, 1.8 ($\times10^{-2}$); (*f*) incoherent Reynolds stress $\langle -u_r v_r\rangle/U_0^2$; levels: $\pm0.5$, $\pm0.4$, $\pm0.3$, $\pm0.2$, $\pm0.1$ ($\times10^{-2}$); (*g*) coherent Reynolds stress $-u_c v_c/U_0^2$; levels: $\pm1.25$, $\pm1.0$, $\pm0.75$, $\pm0.5$, $\pm0.25$ ($\times10^{-2}$); (*h*) coherent strain rate $\langle S\rangle/S_M$: 2.5, 2.0, 1.5, 1.0, 0.5; (*i*) coherent production $\langle P\rangle/(U_0^2 S_M)$; $\langle P\rangle = \langle P_s\rangle + \langle P_n\rangle$; levels: 1.2, 1.0, 0.8, 0.6, 0.4, 0.2 ($\times10^{-2}$); (*j*) coherent shear production $\langle P_s\rangle/(U_0^2 S_M)$; levels: 1.0, 0.8, 0.6, 0.4, 0.2 ($\times10^{-2}$); (*k*) coherent normal production $\langle P_n\rangle/(U_0^2 S_M)$; levels: 0.4, 0.3, 0.2, 0.1, $-0.1$ ($\times10^{-2}$).

the back of the structure C on the opposite side of the wake centreline (figure 10*b*). Since both contributions have the same direction and the outward motion at the back of structure C tends to be smeared owing to jitter away from trigger (i.e. $t = 0$), the contour of the total $v_c$ has a single, transversely elongated shape. Note that at the centre of the aligned structure, (i.e. $t = 0$), $u_c$ curves look symmetric in $y$, and $v_c$ curves look symmetric in $x$, as to be expected. The dotted (vorticity) contour of the aligned (middle) structure in figures 10(*c*, *d*) suggests that the contour level selected to denote the structure boundary is indeed a judicious one as the rotational velocity around the structure is the maximum on this contour; that is, the maxima of $u_c$, $v_c$ fall near this contour.

The incoherent turbulence intensity (figure 10*e*) has its maximum near the centre. There is a marked difference in the contour shape between the front and back regions of the aligned structure B; the intensity at the front is much lower than at the back,

and the lower contour levels encroach past the wake centreline, far more at the front than at the back. This is to be expected because turbulence produced at around the saddle will tend to be accumulated at the back of the structure (discussed later). Thus, the turbulence-intensity distribution is not necessarily useful for defining the structure boundary or even the structure centre. It should be mentioned that contours of turbulence intensity may denote a coherent structure boundary in special situations only (see Fiedler *et al.* 1981). Note that there is a good correspondence between $\langle\omega\rangle$ and $\langle q_r^2\rangle$ contours for the two neighbouring structures A and C. This, along with the fact that the $\langle q_r^2\rangle$ peak values at the centres of A and C are higher than in the aligned structure B should be attributed to the jitter (away from the alignment point $t = 0$) at the centres of A and C where the coherent velocities, $u_c$ and $v_c$, have large spatial variations or gradients (see figure 10*c*, *d*).

We mention in passing that the intermittency signal cannot be an acceptable choice for defining the structure because it is defined on the basis of total instantaneous vorticity and not coherent vorticity. The use of intermittency or turbulence intensity for identifying the large-scale structures is perhaps qualitatively acceptable in the very near field of free shear flows (for example, CC) or a turbulent patch surrounded by non-turbulent fluid like the boundary-layer spot (Wygnanski *et al.* 1976; Cantwell *et al.* 1978) or turbulent puff in transitional pipe flow (Wygnanski, Sokolov & Friedman 1975). Only when the incoherent turbulence is fine scale and uniformly distributed over the structure but zero outside the structure may the centre of the intermittency contour be assumed to coincide with the structure centre. If the incoherent turbulence is non-uniformly distributed spatially, as to be expected because incoherent turbulence is preferentially produced by coherent structures (Hussain 1981*b*, 1983*b*), the peak coherent intermittency may not coincide with the structure centre (Kleis *et al.* 1981). Furthermore, since intermittency in turbulent pipe or channel flow is unity everywhere, intermittency cannot be used to detect coherent structures in these flows; we know that turbulence intensity in these flows does not denote structure boundaries either.

The distribution of the incoherent Reynolds stress (figure 10*f*) is localized to have a peak at around the saddle, and the contour shape is tilted away from the wake centreline, somewhat aligned with the braid or the diverging separatrix at the saddle (discussed later). The peak value of $\langle -u_r v_r\rangle$ is more than twice the maximum time-averaged $-\overline{u_r v_r}$ value but, contrary to the expectation of many, not an order-of-magnitude higher than the time-mean maximum.

The coherent Reynolds stress (figure 10*g*) shows the clover-leaf pattern about the centre, which is a straightforward consequence of the coherent velocity field associated with a vortical motion in a frame advected at $U_c$. The peak value of $-u_c v_c$ is much higher (about 2.5 times) than that of the $\langle -u_r v_r\rangle$-peak. However, it is apparent that the net contribution to the total (time-averaged) Reynolds stress from coherent motion is not significant because negative and positive parts of $u_c v_c$ cancel out their contributions to the time average.

Figure 10(*h*) indicates the occurrence of strong strain rates $\langle S\rangle$ primarily in the saddle region, the maximum being about 2.5 times the local maximum mean shear. Such an intense strain field must be a direct consequence of stretching induced by predominantly spanwise adjacent vortices. This implies that, because there is no significant spanwise vorticity in the saddle region, the vorticity in this region should be aligned mostly in the longitudinal direction. Thus, the successive vortices appear to be connected by 'ribs' – a spanwise array of longitudinal vortices of alternating signs (Hussain 1983*b*). Since ribs are features of plane mixing layers (Konrad 1977;

Bernal 1981; Jimenez *et al.* 1985; Bernal & Roshko 1986) the wake may be viewed in some sense as two opposed mixing layers coupled through large-amplitude three-dimensional contortions (discussed further below).

The contours of the coherent production are shown in figure 10(*i*) for the total production $\langle P\rangle = \langle P_s\rangle + \langle P_n\rangle$, in figure 10(*j*) for the shear production $\langle P_s\rangle$ and in figure 10(*k*) for the normal production $\langle P_n\rangle$. Since both $\langle -u_r v_r\rangle$ and $\langle S\rangle$ have their maxima in the saddle region, the peak of $\langle P_s\rangle$ necessarily occurs in that region. The two peaks on either side of the centre (i.e. at $t = \pm 1.8b/U_c$ and below the wake centreline) have lower values compared to the peak at $t = 0$ owing to jitter away from the alignment point. The $\langle P_n\rangle$-contours are quite different from $\langle S\rangle$, $\langle -u_r v_r\rangle$ or $\langle P\rangle$ contours not only in their shapes, but also in the locations of their peaks. Note that the largest positive peak in $\langle P_n\rangle$ occurs at the back of the structure toward the higher-speed side and that a negative $\langle P_n\rangle$ occurs at the front near the wake centreline. The peak value of $\langle P_n\rangle$ in these coordinates is considerably lower than the peak value of $\langle P_s\rangle$, the ratio of these two maximum values being about 3. Accordingly, the total-production contours (figure 10*i*) closely resemble the shear-production contours (figure 10*k*), a fact also observed in mixing layers (Hussain 1981*a*, *b*). These contours unambiguously demonstrate that the intense production of incoherent turbulence by large-scale coherent structures occurs mostly in the saddle region. The peak value of production is about 5 times that of the time-averaged value. Note that $\langle P_s\rangle$ and $\langle P_n\rangle$ are dependent on the coordinate system chosen while the total production $\langle P\rangle$ is invariant with respect to rotation of axes and thus physically more significant (Hussain 1983*b*).

These remarkable correspondences between the saddle and the locations of the maximum production and strain rate support the notions of Coles (1983) and Hussain (1983*b*) that the basic mechanism of turbulence production is the vortex stretching in the saddle region. In fact, it is noticed that the orientation of inclined contours of $\langle P\rangle$ qualitatively coincides with the direction of stretching of ribs between two predominantly spanwise structures on either side of the wake centreline.

### 5.2. *Mechanism of a plane wake*

Based on the results presented, the coherent-structure topography in a plane wake is conceptually sketched in figure 11(*a*) in a frame of reference moving with the structure advection velocity $U_c$. This sketch provides a reasonable explanation for most experimental data presented here and appears to be realistic, even though it is speculative because of lack of streamwise vorticity data.

As emphasized in the previous section, the saddle is the dynamically most significant point in the flow. The saddle points are denoted by $\times$-marks in figure 11(*a*). The successive spanwise structures produce intense strain in the saddle region (see figure 10*h*) and organize the vorticity of the fluid between them along the diverging separatrix, i.e. the braid, which connects the top of a structure to the bottom of an adjoining structure (Patnaik, Sherman & Corcos 1976). Since production is highest in the braid, the braid cannot be a continuous sheet but is most likely to consist of intermediate-scale longitudinal vortices, i.e. 'ribs', which are separated in the spanwise direction (figure 11*b*). The predominantly spanwise vorticity of the primary (nominally spanwise) structures induces motion of external fluid toward the wake region along the converging separatrix. This flow, directed to the saddles, is denoted by solid arrows in figure 11(*a*). Owing to the motion of outer potential fluid toward the wake centreline (denoted by the longer arrow), the distribution of incoherent-turbulence intensity should have a dip along the structure front (see figure

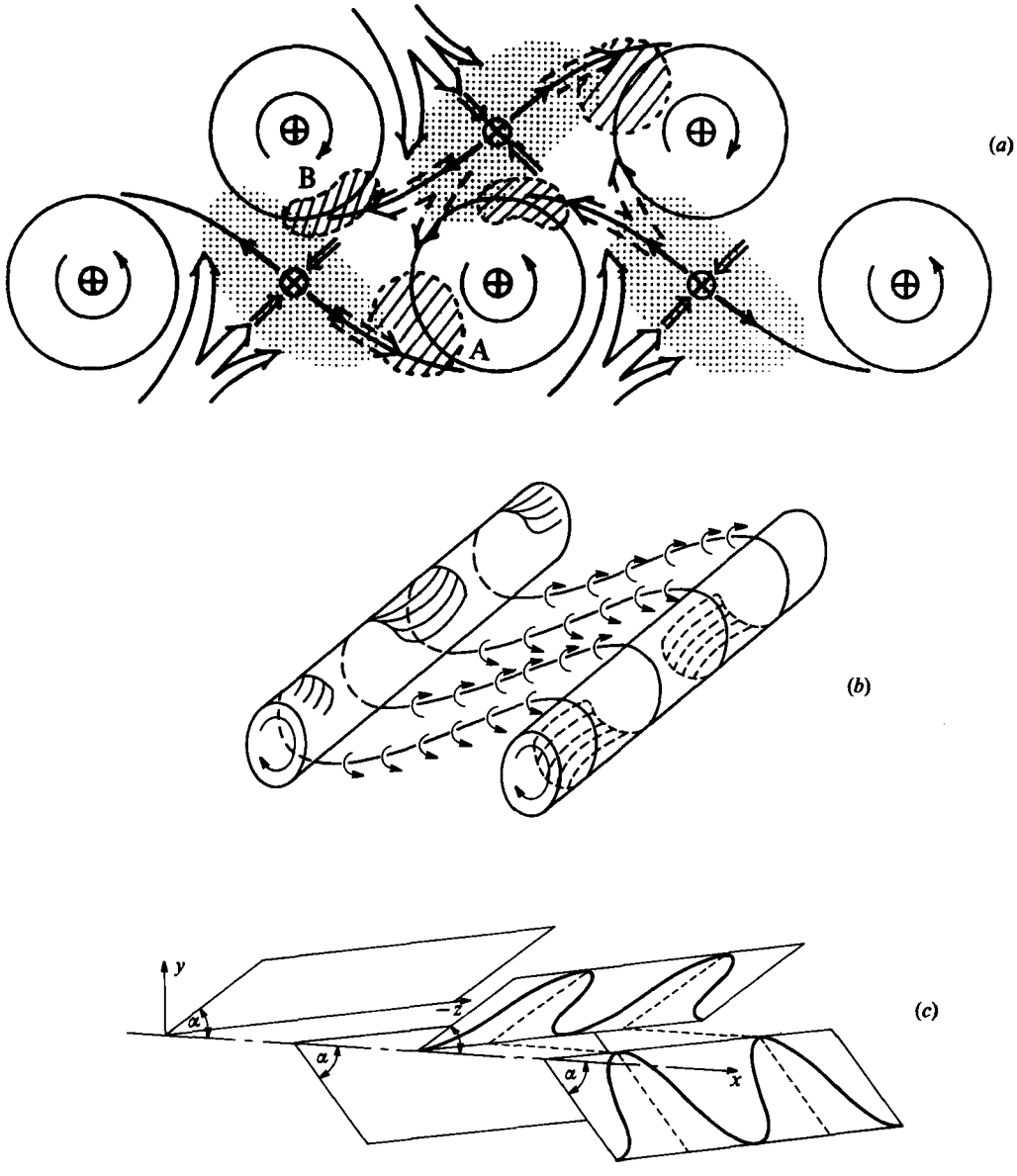


FIGURE 11 (*a–d*). For caption see facing page.

10*e*). This suggests that the braid indeed consists of ribs and irrotational external fluid can percolate through the braid (Hussain 1983*b*), and may explain CC's observation that alternate vortices shed from a cylinder entrain significant amount of fluid from the opposite side of the wake. Thus, the transverse motion of ambient fluid towards the wake does not necessarily imply true entrainment, i.e. the process of acquisition of random vorticity by irrotational fluid. As a result of induction by the counter-rotating longitudinal vortices, or ribs, the rolls (primary coherent structures) will undergo significant spanwise contortions. Thus, the primary coherent structures, or rolls, are indeed three-dimensional.

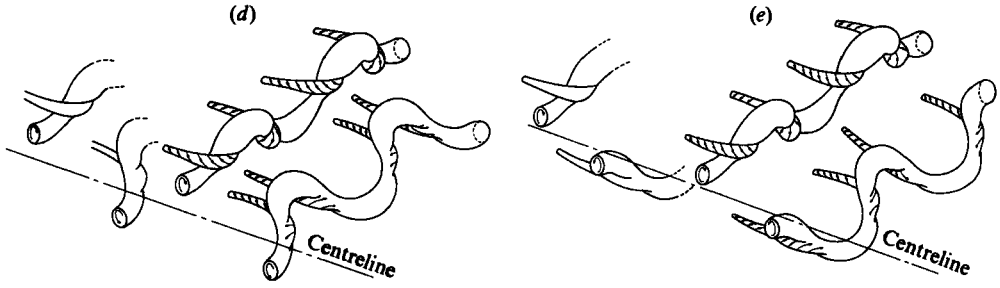


FIGURE 11. Topological feature of coherent structure in the plane wake (conceptual picture); (*a*) a plane cut of the wake: +, centre; ×, saddle point; ⇒, engulfed non-turbulent fluid; ⇒ flow of produced turbulence; ▩ turbulence production (production of incoherent turbulence); ■ turbulence mixing; (*b*) schematic of ribs; (*c*) a simplified schematic of inclinations of contorted rolls. Realistic schematics of the rolls and ribs are given in (*d*) and (*e*). (*d*) Rolls are staggered with respect to each other in the spanwise direction; (*e*) rolls are not staggered with respect to each other.

Fluid advected to saddles picks up the rotation of ribs, and is subjected to the vortex stretching along the diverging separatrix; this is how smaller-scale (incoherent) turbulence is produced in the saddle region. This is why contours of coherent production are elongated and aligned with the braid (see figure 10*i*). The region in which most turbulence production occurs is shown as shaded areas in figure 11(*a*). Due to the inclination of ribs with the $y$-direction, the spinning of ribs generates negative correlation between $u$- and $v$-fluctuations in the saddle region, irrespective of the direction of circulation of the ribs; thus the incoherent Reynolds stress also has a higher value in the saddle region (see figure 10*f*). Note that turbulence-production contours protrude into the primary structure on the wake-centreline side (figure 10*i*), which is not unexpected (Tennekes & Lumley 1972) from the considerations of intense strain rate in this region, as seen in figure 10(*h*). Another possibility is that the protruded production contours are an artifact caused by the spanwise undulation of rolls induced by the ribs, because ensemble averaging without spanwise alignment cannot account for displacement due to the spanwise undulation.

The turbulence produced is continuously advected into the rolls, causing a higher incoherent-turbulence intensity near the structure centre and also toward the back of the structure (see figure 10*e*) these paths are shown by broken arrows in figure 11(*a*). The strong outward motion together with the turbulence intensity on the back side of the structure (figures 10*d*, *e*) suggests an important role of the back (as opposed to the front) of the structure in transporting smaller-scale turbulence to the outer edge of the wake.

We deduce that the most effective mixing occurs in the hatched areas A and B (in figure 11*a*) because of the direct interaction between the rib fluid with longitudinal vorticity and the roll fluid with mostly spanwise vorticity, presumably producing stronger three-dimensional vorticity fluctuations. Furthermore, owing to the combined effects of this interaction and the presence of a high turbulence intensity at the back of the structure, mixing in the hatched area A will be greater than that in B. Although the present measurements cannot evaluate the actual extent of mixing, we maintain that most turbulence mixing occurs in highly localized regions. The quantitative measurement of mixing rate of Konrad (1977) in a plane mixing layer and a flat-plate wake shows that much of the engulfed fluid, even within the wake, is still in an unmixed state; however, he did not consider where the dominant mixing process occurs with respect to large-scale structures.

From these results and extensive studies of axisymmetric and plane mixing layers by us and others, a qualitative picture of the dynamics of a plane turbulent wake is emerging. The wake can be viewed as a superposition of two coherent vorticity layers consisting of large-scale nominally spanwise vortex rolls of opposite circulations; yet these two layers are strongly influenced by each other and coupled through large three-dimensional contortions. Figures 11 (*d*, *e*) show two possible configurations of the wake structure. The structures on the two sides are inclined with the flow direction. This is depicted by the simple schematic in figure 11 (*c*), which also shows that the contortions are staggered in the spanwise direction (corresponding to figure 11*d*). A schematic like figure 11 (*c*) to correspond to figure 11 (*e*) is not shown but is not hard to imagine. The coupling is indeed complicated and even involves some fluid exchange between the two layers (see broken arrows in figure 11*a*). The successive rolls (of the same sign on either side of the centreline) are connected to each other via intermediate-scale, coherent substructures, i.e. ribs, characterized by strong longitudinal vorticity. Adjacent ribs have longitudinal vorticities of opposite sign so that there is no net circulation in the longitudinal planes (see figure 11*b*). Also, the rolls are distorted in the spanwise direction. The stretching of the ribs by adjacent (nominally spanwise) rolls would increase the spinning of ribs (but countered by viscous effects) and thus causing higher velocity fluctuations normal to the ribs; this appears to be a fundamental mechanism of turbulence production (Hussain 1983*b*). Note that this constitutes a marked contrast to the well-accepted notion that turbulence production first occurs in the longitudinal ($u$) component, which is then converted into transverse ($v$ and $w$) components by the influence of static pressure fluctuations (see, for example, Tennekes & Lumley 1972). The significant amount of turbulence produced in the ribs is drained away from the saddle region and accumulated in the rolls. Velocity fluctuations produced at the ribs consist of essentially two-dimensional, spinning motion and thus are not truly turbulence and produce very little mixing. (Note that in coordinates with $x$ aligned with the free-stream direction, the ribs are inclined to the $x$-direction; one can thus say that production involves simultaneous generation of $u$, $v$ and $w$.) When the rib fluid with streamwise vorticity encounters roll fluid with predominantly spanwise vorticity, the interaction of orthogonal vorticities produces smaller-scale, three-dimensional vorticity fluctuations and hence promotes substantial mixing. This notion was proposed earlier by Hussain (1983*b*).

Next, we would qualitatively consider the downstream evolution of the wake structure, primarily based on the instantaneous behaviour of coherent vorticity. As discussed above, adjacent rolls stretch ribs between them and produce turbulence which is drained away from ribs and is deposited into the structure cores. This newly added turbulence partly counters turbulence decay and maintains the turbulence energy in the rolls. Thus, the dynamics of a coherent structure seems to involve a mechanism of its own survival. Hussain (1983*b*) proposed this as a general mechanism for all turbulent shear flows.

Then, why do large-scale structures in the wake appear to eventually decay (presumably at about 80 diameters downstream in the present wake)? One of the plausible answers may be that with increasing $x$, the driving force rotating the roll structures weakens owing to the decrease of structure strength and thus the stretching of ribs weakens too so that the resulting production is insufficient to replenish the decay completely. However, instantaneous vorticity maps (see figures 1*a–g*) suggest that this decay is more a result of evolution of three-dimensionality and breakdown process (like a partial tearing) than viscous decay. Indeed, our

subsequent experiments (Hayakawa & Hussain 1986) have shown significantly low spanwise coherence of rolls as well as the occurrence of many transverse vorticity concentrations even at $x/d = 20$. (This new experiment measured not only the spanwise vorticity simultaneously in two different $(x, y)$-planes but also the transverse vorticity component in either one $(x, z)$-plane or simultaneously in two $(x, z)$-planes, using several combinations of two X-wire rakes.) Furthermore, large-scale transverse vorticity ($\omega_y$) concentrations often occur in pairs with opposite circulations occurring adjacently, suggesting that the spanwise structure is distorted in a form like a horseshoe-type vortex. As we suggested, this deformation might be due to the strong induction of ribs. Such three-dimensionality and wandering of structures of various sizes and strengths promote disorganization of the wake.

Another important mechanism in viscous turbulent flows, which may be relevant to disorganization of the wake structure, is the so-called cut-and-connect interaction of vortex filaments (Oshima & Asaka 1977; Takaki & Hussain 1985). This is a mechanism of generation of smaller-scale coherent structures via cross-linking of vortex filaments and may be a dominant factor in both decay and formation mechanisms. It is our contention that this mechanism occurs in all turbulent flows, is central to mixing and noise phenomena, and is crucial to the production of helicity and enstrophy cascade (Hussain 1986). We believe that the originally formed spanwise rolls, deformed by ribs and spanwise instability, result in smaller-scale structures through the cut-and-connect process. This may be the major cause of the breakdown phenomena in the wake and suggests that as the wake evolves, not all initial spanwise structures survive as identified entities but break down into three-dimensional, intermediate-scale structures.

The emerging disorganized wake appears to have its own instability, generating newer structures (Taneda 1959; Cimbala 1984), and this instability process could be the same as in the case of a porous-plate wake. However, we also suggest another possible mechanism: some structures never decay but may even get energized (say, via pairing) while others decay owing to tearing so that the surviving structures readjust their increased spacing. This interpretation of structure evolution is different from the notion of a 'growth–decay–renewal cycle' (Townsend 1979) wherein older structures are presumed to completely decay and then newer structures evolve as a result of instability of the locally structureless wake.

Perhaps, the best-known (even widely accepted ) organized structure in the far-field wake is the so-called double-roller eddy which has been persistently proposed by the Cambridge school on the basis of longitudinal velocity correlation measurements (Townsend 1956; Grant 1958; Savill 1983; Mumford 1983). We consider that such a column-like transverse structure extending over both sides of the wake centreline would not be a dominant structure that occurs instantaneously. Instead, it seems more likely that the double-roller-type picture is a simple consequence of the horseshoe-type contortions of rolls on either side of the wake. Structures across the centreline may link up through the cut-and-connect interaction, but this is not likely to be frequent. Time-average correlation of these horseshoe-type-contortion vortices is quite likely to resemble that of double-roller structures.

## 6. Concluding remarks

A comprehensive effort has been devoted to develop a suitable conditional-sampling scheme for educing coherent structures in fully turbulent flows. This scheme is based on the intrinsic property of coherent structures, i.e. coherent vorticity, and is

independent of either periodic excitation or an auxiliary reference or detection signal for trigger. A linear array of X-wires is used to obtain instantaneous (large-scale) spanwise vorticity maps in the plane of the array and the mean-flow direction.

The eduction involves careful selection of (smoothed) vorticity concentrations from these maps and then obtaining ensemble averages. The smoothed vorticity is used to identify the true (hidden) structure centre but the original, unsmoothed signals are then used to obtain ensemble averages to characterize coherent structures and incoherent turbulence. Large-scale vortical structures have been successfully educed in the intermediate region of a cylinder wake up to the downstream distance of $40d$, that being far beyond the region covered by earlier measurements. Our technique is free from jitter which, we believe, has significantly smeared earlier measurements. Since structures undergo decay in the intermediate region and new structures form farther downstream (the formation mechanism remains controversial), this region seems optimal for demonstrating the success of coherent-structure eduction in the fully turbulent wake. The structures farther downstream may emerge as a result of local instability or as a result of interactions of existing structures; which of these two is more predominant is unclear.

In principle, our eduction scheme is applicable to any shear flow, even in their self-preserving regions, as long as dominant coherent structures exist in the flow. We continue to maintain that implicit with the coherent-structures approach to turbulence is the existence of dominant or preferred modes; if a flow has a variety of coherent structures, the coherent-structures approach to turbulence is not useful.

The success of the present scheme is primarily due to the detection technique which enabled us to identify the coherent structure centres with the least ambiguity and to minimize the otherwise unavoidable smearing caused by the structure jitter. The rather strict eduction process employed here may lead one to raise the question that the educed structure might be an artifact of the sampling scheme. However, a coherent structure must be educed via ensemble averaging, and the ensemble-averaged properties must be obtained for a selective combination of structure measures like strength, size, etc. We have selected the dominant, typical structure out of many realizations in the flow where the large-scale vortical structures were identified by instantaneous vorticity contours. Thus, the eduction and enhancement process works not to smear or deform but to sharpen the structure details. In fact, the eduction technique has been validated by applying it to the case of the 'preferred mode' of a circular jet, where the coherent-structure details are known independently by phase-locked measurements of periodically excited structures.

The topological features of coherent structure have been discussed on the basis of data which are more detailed and accurate than has been possible heretofore. The results clearly indicate the dynamical significance of the saddle region where most smaller-scale turbulence is produced by the stretching of rib vortices along the braid (the diverging separatrix) by the large-scale spanwise structures.

The limitations of the present measurement technique restrict our description of flow physics to only a spanwise plane view of the coherent structures. Nevertheless, we conclude from the data that the saddle region consists of intermediate-scale longitudinal vortex structures (i.e. ribs) which are aligned along the diverging separatrix and are characterized by longitudinal vorticity. The increasing scatter of smoothed vorticity contours with increasing $x$ is mainly due to the wandering of individual structures associated with the evolution of strong three-dimensionality, which has been confirmed by our subsequent experiment using several combinations of X-wire rakes. All these suggest that simultaneous three-dimensional measurement

is needed to obtain further insights into the structure details. This will require sophisticated conditional sampling with three-dimensional detection which at present is beyond the available technology and laboratory computer capability. Perhaps, image processing, including pulsed laser holography or NMR or ESR imaging velocimetry, would be necessary to obtain adequate three-dimensional spatial details of coherent structures and their evolution. Pending development of these sophisticated measurement techniques, we have relied on the two-dimensional measurements reported here to speculate on the qualitative features of the wake coherent structure, with emphasis on their three-dimensionality owing to ribs and associated spanwise contortion of what are commonly assumed to be two-dimensional spanwise roll structures.

Finally, it cannot be overlooked that, in spite of the fine-tuned eduction process, there is a non-negligible amount of jitter which increases with increasing distance away from the alignment point or trigger. This rather discouraging aspect raises questions regarding the validity of data based on a reference signal at a far upstream position or even at the outer edge of the shear flow. In other words, the minimum requirement for the detection of coherent structures in the fully developed turbulent regime must be a conditional sampling based on a flow property identifying the structure itself. This is what has been done in this paper – coherent structures have been educed from local vorticity signals.

The authors are grateful to Dr Jin Tso for his collaborative work in the early phase of this study, and to Drs S. J. Kleis and H. S. Husain for their helpful support in experiment and data analyses, and to Mr A. Degani for a review of the manuscript. M.H. would like to thank Professors Y. Kobashi and S. Iida and also Dr M. Ichijo and Mr Y. Nozaki for continuous encouragement from Japan during his stay at the University of Houston.

This work was supported by the Office of Naval Research under the grant N00014-85-K-0126 monitored by Dr M. M. Reischman.

## REFERENCES

Bernal, L. P. 1981 The coherent structure of turbulent mixing layers. I. Similarity of primary vortex structure. II. Secondary streamwise vortex structure. Ph.D. thesis, California Institute of Technology.

Bernal, L. P. & Roshko, A. 1986 *J. Fluid Mech.* **170**, 499.

Blackwelder, R. F. & Kaplan, R. E. 1976 *J. Fluid Mech.* **76**, 89.

Boisson, H. C. 1983 Dévelopment de structures organizées turbulentes à travers l'exemple du sillage d'un cylindre circulaire. Ph.D. thesis, IMF, Toulouse, France.

Breidenthal, R. E. 1980 *Phys. Fluids* **23**, 1929.

Browand, F. K. 1980 Lecture at APS Meeting, Cornell University.

Browand, F. K. & Troutt, T. R. 1985 *J. Fluid Mech.* **158**, 489.

Browand, F. K. & Weidman, P. D. 1976 *J. Fluid Mech.* **76**, 127.

Brown, G. L. & Roshko, A. 1974 *J. Fluid Mech.* **64**, 775.

Bruun, H. H. 1977 *J. Fluid Mech.* **83**, 641.

Cantwell, B. & Coles, D. 1983 *J. Fluid Mech.* **136**, 321.

Cantwell, B., Coles, D. & Dimotakis, P. 1978 J. Fluid Mech. **87**, 641

Castro, I. 1971 *J. Fluid Mech.* **46**, 599.

Cimbala, J. M. 1984 Large structure in the far wakes of two dimensional bluff bodies. Ph.D. thesis, California Institute of Technology.

Cimbala, J. M., Nagib, H. & Roshko, A. 1981 *Bull. Am. Phys. Soc.* **26**, 1256.

COLES, D. 1981 *Proc. Ind. Acad. Sci.* (*Engng Sci.*) **4**, 111.

COLES, D. 1983 *Turbulence and Chaotic Phenomena in Fluids* (ed. T. Tatsumi), p. 397. North-Holland.

CROW, C. & CHAMPAGNE, F. H. 1971 *J. Fluid Mech.* **48**, 547.

DESRUELLE, D. 1983 Beyond the Kármán vortex street. M.S. thesis, Illinois Institute of Technology.

DURGIN, W. & KARLSSON, B. 1971 *J. Fluid Mech.* **48**, 507.

FIEDLER, H. E., DZIOMBA, B., MENSING, P. & RÖSGEN, T. 1981 In *Role of Coherent Structures in Modelling Turbulence and Mixing* (ed. J. Jimenez). Lecture Notes in Physics, vol. 136, p. 219. Springer.

GERRARD, H. 1966 *J. Fluid Mech.* **25**, 143.

GRANT, H. L. 1958 *J. Fluid Mech.* **4**, 149.

GUPTA, A., LAUFER, J. & KAPLAN, R. 1971 *J. Fluid Mech.* **50**, 493.

HAYAKAWA, M. & HUSSAIN, A. K. M. F. 1985 *Turbulent Shear Flows V*, p. 4.38. Cornell University (also *Rep.* FM-20, University of Houston).

HAYAKAWA, M. & HUSSAIN, A. K. M. F. 1986 *Proc. 3rd Asian Cong. Fluid Mech.* (ed. T. Matsui), p. 206. H. Sato.

HAYAKAWA, M., TSO, J., KLEIS, S. J. & HUSSAIN, A. K. M. F. 1983 *Bull. Am. Phys. Soc.* **28**, 1370.

HUSAIN, H. S. 1984 An experimental investigation of unexcited and excited elliptic jets. Ph.D. thesis, University of Houston.

HUSSAIN, A. K. M. F. 1981*a* In *Role of Coherent Structures in Modelling Turbulence and Mixing* (ed. J. Jimenez). Lecture Notes in Physics, vol. 136, p. 252. Springer.

HUSSAIN, A. K. M. F. 1981*b* *Proc. Ind. Acad. Sci.* (Eng. Sc.) **4**, 129.

HUSSAIN, A. K. M. F. 1983*a* *Phys. Fluids* **26**, 2816.

HUSSAIN, A. K. M. F. 1983*b* *Turbulence and Chaotic Phenomena in Fluids* (ed. T. Tatsumi), p. 453. North-Holland.

HUSSAIN, A. K. M. F. 1986 *J. Fluid Mech.* **173**, 303.

HUSSAIN, A. K. M. F. & CLARK, A. R. 1981 *J. Fluid Mech.* **104**, 493.

HUSSAIN, A. K. M. F. & ZAMAN, K. B. M. Q. 1980 *J. Fluid Mech.* **101**, 493.

HUSSAIN, A. K. M. F. & ZAMAN, K. B. M. Q. 1982 *Rep.* FM-14, University of Houston (also *J. Fluid Mech.* **159**, 85 (1985)).

HUSSAIN, A. K. M. F. & ZAMAN, K. B. M. Q. 1985 *J. Fluid Mech.* **159**, 85.

JIMENEZ, J., COGOLLOS, M. & BERNAL, L. P. 1985 *J. Fluid Mech.* **152**, 125.

KEFFER, J. 1965 *J. Fluid Mech.* **22**, 135.

KLEIS, S. J., HUSSAIN, A. K. M. F. & SOKOLOV, M. 1981 *J. Fluid Mech.* **111**, 87.

KLINE, S. J., REYNOLDS, W. C., SCHRAUB, F. A. & RUNSTADLER, P. W. 1967 *J. Fluid Mech.* **30**, 741.

KONRAD, J. H. 1977 An experimental investigation of mixing in two-dimensional turbulent shear flows with applications to diffusion-limited chemical reactions. Ph.D. thesis, California Institute of Technology.

KUNEN, J. M. G., OOMS, & VINK, P. J. J. 1983 *Symp. Turbulence*, p. 37. University of Missouri-Rolla.

MATSUI, T. & OKUDE, M. 1981 *Turbulence in Liquids*, p. 303. University of Missouri-Rolla.

MATSUI, T. & OKUDE, M. 1983 In *Structure of Complex Turbulent Shear Flow* (ed. R. Dumas & L. Fulachier), p. 156. Springer.

METCALFE, R., HUSSAIN, A. K. M. F., MENON, S. & HAYAKAWA, M. 1987 *Fifth Symp. Turbulent Shear Flow*, Vol. 5 (ed. F. Durst *et al.*), p. 110, Springer.

MUMFORD, J. C. 1983 *J. Fluid Mech.* **137**, 447.

NISHIOKA, M., ASAI, M. & IIDA, S. 1981 In *Transition and Turbulence* (ed. R. E. Meyer), p. 113. Academic.

NISHIOKA, M. & SATO, H. 1978 *J. Fluid Mech.* **89**, 49.

OSHIMA, Y. & ASAKA, S. 1977 *J. Phys. Soc. Japan* **42**, 708.

PATNAIK, P. C., SHERMAN, F. S. & CORCOS, G. M. 1976 *J. Fluid Mech.* **73**, 215.

PERRY, A. E., CHONG, M. S. & LIM, T. T. 1982 *J. Fluid Mech.* **116**, 77.

PERRY, A. E. & WATMUFF, J. H. 1981 *J. Fluid Mech.* **103**, 33.

ROSHKO, A. 1954 *NASA TN* 3169.

SATO, H. 1983 *Proc. 2nd Asian Cong. Fluid Mech.* (ed. T. Deyan), p. 7. Beijing, China: Science.

SAVILL, A. M. 1983 In *Structure of Complex Turbulent Shear Flow* (ed. R. Dumas & L. Fulachier), p. 185. Springer.

SREENIVASAN, K. R. & NARASIMHA, R. 1982 *Trans. ASME* I: *J. Fluids Engng* **104**, 167.

TAKAKI, R. & HUSSAIN, A. K. M. F. 1985 *Fifth Symp. Turbulent Shear Flow*, p. 3.19. Cornell University.

TANEDA, S. 1959 *J. Phys. Soc. Japan* **14**, 843.

TENNEKES, H. & LUMLEY, J. L. 1972 *A First Course in Turbulence.* MIT Press.

TOWNSEND, A. A. 1956 *The Structure of Turbulent Shear Flow.* Cambridge University Press.

TOWNSEND, A. A. 1979 *J. Fluid Mech.* **95**, 515.

TRITTON, D. J. 1959 *J. Fluid Mech.* **6**, 547.

TSO, J. 1983 Coherent structures in a fully-developed turbulent axisymmetic jet. Ph.D. thesis, Johns Hopkins University.

WINANT, C. D. & BROWAND, F. K. 1974 *J. Fluid Mech.* **63**, 237.

WLEZIEN, R. 1981 The evolution of the low-wavenumber structure in a turbulent wake. Ph.D. thesis, IIT, Chicago.

WYGNANSKI, I., CHAMPAGNE, F. & MARASLI, B. 1986 *J. Fluid Mech.* **168**, 31.

WYGNANSKI, I., SOKOLOV, M. & FRIEDMAN, D. 1975 *J. Fluid Mech.* **69**, 283.

WYGNANSKI, I., SOKOLOV, M. & FRIEDMAN, D. 1976 *J. Fluid Mech.* **78**, 785.

YULE, A. J. 1978 *J. Fluid Mech.* **89**, 413.

ZAMAN, K. B. M. Q. & HUSSAIN, A. K. M. F. 1981 *J. Fluid Mech.* **112**, 379.

ZAMAN, K. B. M. Q. & HUSSAIN, A. K. M. F. 1984 *J. Fluid Mech.* **138**, 325

ZILBERMAN, M., WYGNANSKI, E. & KAPLAN, R. E. 1977 *Phys. Fluids Suppl.* **20**, S258.

ZDRAVKOVICH, M. M. 1968 *J. Fluid Mech.* **32**, 339.